





## Article

# A Seven-Parameter Spectral/*hp* Finite Element Model for the Linear Vibration Analysis of Functionally Graded Shells with Nonuniform Thickness

Carlos Enrique Valencia Murillo , Miguel Ernesto Gutierrez Rivera \* , Nicolas Flores Samano   
and Luis David Celaya Garcia 

Department of Mechanical Engineering, University of Guanajuato, Salamanca 36885, Guanajuato, Mexico; ce.valenciamurillo@ugto.mx (C.E.V.M.); n.floressamano@ugto.mx (N.F.S.); ld.celayagarcia@ugto.mx (L.D.C.G.)  
\* Correspondence: miguel.gutierrez@ugto.mx

**Abstract:** This contribution presents a finite element shell model capable of performing linear vibration analyses of shell-type structures made of functionally graded material (FGM). The model is based on the seven-parameter spectral/*hp* finite element formulation, which allows the analysis of FG shells of either uniform or nonuniform thickness. Equations of motion are derived using the Hamilton's principle and the material properties of the constituents are considered to follow a power-law volume distribution through the thickness direction. The verification of the present model is carried out by comparing with numerical results available in the literature, and with numerical simulations performed in a commercial software. To demonstrate the capabilities of the present formulation, the free vibration response of different shell structures, with nonuniform thickness, to the variation of the geometrical parameters (e.g., radius-to-thickness ratio) and the mechanical properties is reported.

**Keywords:** functionally graded material; seven-parameter shell formulation; finite element model; natural frequencies; numerical results; thickness variation



**Citation:** Valencia Murillo, C.E.; Gutierrez Rivera, M.E.; Flores Samano, N.; Celaya Garcia, L.D. A Seven-Parameter Spectral/*hp* Finite Element Model for the Linear Vibration Analysis of Functionally Graded Shells with Nonuniform Thickness. *Appl. Sci.* **2023**, *13*, 11540. <https://doi.org/10.3390/app132011540>

Academic Editor: Victor Franco Correia

Received: 26 September 2023

Revised: 17 October 2023

Accepted: 20 October 2023

Published: 21 October 2023



**Copyright:** © 2023 by the authors. Licensee MDPI, Basel, Switzerland. This article is an open access article distributed under the terms and conditions of the Creative Commons Attribution (CC BY) license (<https://creativecommons.org/licenses/by/4.0/>).

## 1. Introduction

The extensive field of engineering applications in diverse industries (e.g., automotive, nautical, aeronautics, aerospace) in conjunction with the continuously more demanding design requirements has led to the development of advanced materials capable of addressing their needs, improving their performance, or eliminating deficiencies of conventional materials. For instance, composite materials allow a weight reduction in structural members or machine components without compromising the design requirements. Among these advanced materials, an interesting material known as functionally graded material (FGM) is found, which is basically a material with a variation of mechanical properties along one direction or more. In the literature, it is well known that FGMs were introduced to overcome the limitations of composites, such as delamination at high temperatures due to stress concentrations at interfaces of the composite [1,2]. The concept of FGM was introduced in the 1980s by a group of scientists in Japan [1,3,4]. The available computational resources nowadays, which are very powerful tools for engineers, and the complexities involved in the modeling of new materials have motivated the development of numerical models to predict their mechanical behavior. In the last three decades, researchers have shown increasing interest in the area of FGMs.

As mentioned earlier, the functionally graded materials present—in the most general case—a variation of properties through various directions (e.g., along thickness coordinate), and they are usually composed of a mixture of two materials. Therefore, this variation made the FGM a heterogeneous material; due to this fact, different mathematical models,

also known as homogenization schemes [5], have been used to evaluate the effective properties of the FGMs, and the gradation of the volume fraction. Several analytic approaches have been proposed, like self-consistent estimates, Mori–Tanaka scheme, Vegard’s rule, composite sphere assemblage model, composite cylindrical assemblage model, the simplified strength of materials method, the method of cells, and micromechanical models [5–7]. Some models that have attracted more attention are Voigt’s mixture rule, Mori–Tanaka scheme, and self-consistent models [8]. Generally, the rule of mixture and Mori–Tanaka schemes are used by researchers [3].

The present literature review is limited to those works reporting the free vibration analysis of functionally graded (FG) shell structures, specially those considering a variation of the material properties through the thickness and using a power-law volume distribution of the constituents. Despite this, during the review, free vibration analyses of FG plates with uniform thickness were also found in the works [9–17], while vibration analyses of FG plates with variable thickness can be found in [18–20].

Studies related to shells of uniform thickness were presented by Matsunaga [21], Tornabene, Viola and Inman [22], Tornabene and Viola [23], Iqbal, Naeem and Sultana [24], Neves et al. [25], Su et al. [26,27], Su, Jin and Ye [28], Torabi and Ansari [29], Ersoy, Mercan and Civalek [30], Brischetto [31], Pham et al. [32], Moita et al. [33], Zannon et al. [34], and Bagheri et al. [35]. In the aforementioned works, the formulations are based on different theories such as first-order shear deformation theory (FSDT), third-order shear deformation theory (TSDT), higher-order shear deformation theory (HSDT), wave propagation approach, Carrera’s unified formulation, and three-dimensional elasticity theory.

Analysis of the free vibration of stepped FG shells was reported by Li et al. [36] and Gong et al. [37]. Formulations considering the variation of the shell thickness were presented by Tornabene, Fantuzzi, and Baccocchi [38] for the analysis of FG laminated free-form doubly-curved shells and panels, and by Tornabene et al. [39] for FG sandwich shell structures. However, they used different schemes to model the variation of the mechanical properties, such as four-parameter power-law, Weibull, and exponential distributions.

Furthermore, in the literature, the modeling of FG shell type structures or FG plates by means of commercial finite element codes is also reported. Examples of models using ANSYS are the works of Rao, Blessington, and Tarapada [40], Mouli et al. [41], and Marzavan and Nastasescu [42]. In this regard, Burlayenko et al. [43] used a three-dimensional brick finite element available in ABAQUS to model the free vibration of FG sandwich plates.

In the literature, several works related to the seven-parameter finite element formulation can be found [44–48]. However, to date, the implementations of this formulation were devoted to performing different analyses than the modal analysis of FG shell structures with nonuniform thickness.

The main aim of this work is to extend the finite element analysis previously presented in [49] for the modeling of shell-type structures made of FGMs; that is, to take into account the FGM behavior in the seven-parameter finite element formulation in order to determine the natural frequencies and vibration modes of arbitrary FG shell structures with uniform and nonuniform thicknesses. Moreover, due to the few results available in the literature for FG shell-like structures with variable thickness, a user-defined routine to model these type of structures by means of the commercial code ANSYS mechanical APDL is developed and used to compare the results of the present finite element model. In addition, the routine performance is verified using natural frequencies of FG structures with constant thickness reported in the literature.

## 2. Theoretical Formulation

Since the present work is an extension of the finite element model presented in [49], the most relevant aspects related to the formulation are given below, and a more detailed explanation can be found in the previously mentioned work. In Figure 1, the three-dimensional (3D) geometry of the shell element  $\Phi$  and the discretization of the mid-surface  $\Omega$  are shown; the main idea to model the 3D domain is to represent it by means of its mid-surface. In this

case, Figure 1 illustrates the discretization of the shell's mid-surface using spectral nodes for an element with polynomial order  $p = 4$ .

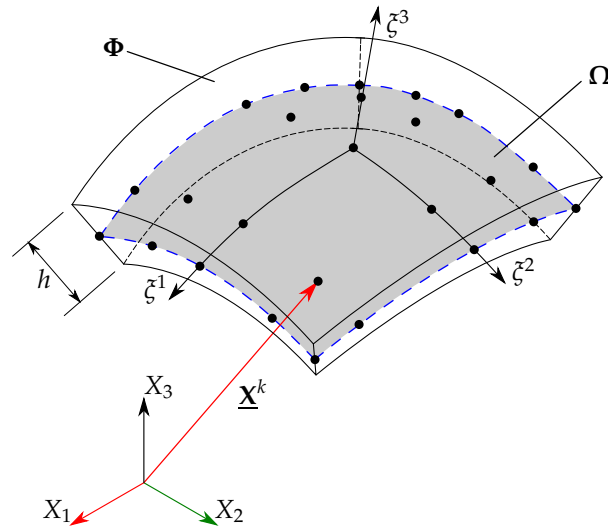


Figure 1. Mid-surface and spectral nodes of a shell element.

2.1. Geometrical Parameters

The position vector of a typical point in the element  $\Phi$  can be approximated as

$$\mathbf{X} = \sum_{k=1}^q \psi_k(\zeta_1, \zeta_2) \left( \mathbf{X}^k + \zeta^3 \frac{h}{2} \mathbf{n}^k \right), \tag{1}$$

where  $\psi_k(\zeta^1, \zeta^2)$  is the  $k$ -th two-dimensional (2D) Lagrange interpolation function of order  $p$ ,  $\mathbf{X}^k$  is the position vector,  $\mathbf{n}^k$  is the unit normal vector of the  $k$ -th spectral node, and  $h$  denotes the thickness in the  $k$ -th spectral node position, so the thickness variation can be easily considered. The total number of nodes per element is  $q = (p + 1)(p + 1)$ .

Additionally, a set of covariant basis vectors for each point in the element must be defined:

$$\mathbf{g}_i = \frac{\partial \mathbf{X}}{\partial \zeta^i} \equiv \mathbf{X}_{,i} \quad i = 1, 2, 3. \tag{2}$$

A differential line element in the typical shell element, in terms of the curvilinear coordinates, can be expressed as

$$\begin{Bmatrix} dX_1 \\ dX_2 \\ dX_3 \end{Bmatrix}^T = \begin{Bmatrix} d\zeta^1 \\ d\zeta^2 \\ d\zeta^3 \end{Bmatrix}^T \begin{bmatrix} \frac{\partial X_1}{\partial \zeta^1} & \frac{\partial X_2}{\partial \zeta^1} & \frac{\partial X_3}{\partial \zeta^1} \\ \frac{\partial X_1}{\partial \zeta^2} & \frac{\partial X_2}{\partial \zeta^2} & \frac{\partial X_3}{\partial \zeta^2} \\ \frac{\partial X_1}{\partial \zeta^3} & \frac{\partial X_2}{\partial \zeta^3} & \frac{\partial X_3}{\partial \zeta^3} \end{bmatrix} = \{d\zeta\}^T [\mathbf{J}], \tag{3}$$

where  $[\mathbf{J}]$  is the Jacobian matrix with determinant  $J$ . In conjunction with the covariant basis vectors, a contravariant set of basis vectors  $\mathbf{g}^i$  is defined, as follows:

$$\mathbf{g}^1 = \frac{\mathbf{g}_2 \times \mathbf{g}_3}{J}, \quad \mathbf{g}^2 = \frac{\mathbf{g}_3 \times \mathbf{g}_1}{J}, \quad \mathbf{g}^3 = \frac{\mathbf{g}_1 \times \mathbf{g}_2}{J}.$$

### 2.2. Displacement Field

The displacement field of the seven-parameter formulation considered in this work is given by [46,47]

$$\mathbf{u}(\mathbf{X}, t) = \underline{\mathbf{u}}(\zeta^\alpha, t) + \zeta^3 \frac{h}{2} \boldsymbol{\varphi}(\zeta^\alpha, t) + \left(\zeta^3\right)^2 \frac{h}{2} \boldsymbol{\Psi}(\zeta^\alpha, t), \tag{4}$$

where

$$\underline{\mathbf{u}}(\zeta^\alpha, t) = \underline{u}_i(\zeta^\alpha, t) \hat{\mathbf{E}}_i, \quad \boldsymbol{\varphi}(\zeta^\alpha, t) = \varphi_i(\zeta^\alpha, t) \hat{\mathbf{E}}_i, \quad \boldsymbol{\Psi}(\zeta^\alpha, t) = \Psi(\zeta^\alpha, t) \underline{\mathbf{n}}(\zeta^\alpha),$$

Here,  $\hat{\mathbf{E}}_i$  is a unit vector in direction  $i$  of the Cartesian coordinate system  $X_1 X_2 X_3$ ; therefore, the subindex  $i$  takes the values of 1, 2, and 3.

In Equation (4), the vector  $\underline{\mathbf{u}}(\zeta^\alpha, t)$  is associated with the mid-surface displacements in the three directions,  $\boldsymbol{\varphi}(\zeta^\alpha, t)$  is the difference vector which gives the change in the mid-surface director, and the vector  $\boldsymbol{\Psi}(\zeta^\alpha, t)$  is defined by scaling the normal vector  $\underline{\mathbf{n}}$  with the seventh parameter  $\Psi$ , which denotes the thickness stretch and mitigates the Poisson’s locking phenomena that appear in the six-parameter formulation [47,48].

### 2.3. Strains

The strains in the element are obtained by considering only the linear part of the Green–Lagrange strain tensor, and are given by

$$\mathbf{E} = \frac{1}{2} (\mathbf{u}_{,i} \cdot \mathbf{g}_j + \mathbf{g}_i \cdot \mathbf{u}_{,j}) \mathbf{g}^i \otimes \mathbf{g}^j, \tag{5}$$

which can be expressed in their covariant components as [50]

$$\mathbf{E} = E_{\alpha\beta} \mathbf{g}^\alpha \otimes \mathbf{g}^\beta + E_{\alpha 3} \mathbf{g}^\alpha \otimes \mathbf{g}^3 + E_{3\alpha} \mathbf{g}^3 \otimes \mathbf{g}^\alpha + E_{33} \mathbf{g}^3 \otimes \mathbf{g}^3, \tag{6}$$

where, considering only the linear terms associated with the thickness coordinate, the covariant components are

$$E_{\alpha\beta} = \varepsilon_{\alpha\beta}^{(0)}(\zeta^\alpha, t) + \zeta^3 \varepsilon_{\alpha\beta}^{(1)}(\zeta^\alpha, t), \tag{7}$$

$$E_{\alpha 3} = \varepsilon_{\alpha 3}^{(0)}(\zeta^\alpha, t) + \zeta^3 \varepsilon_{\alpha 3}^{(1)}(\zeta^\alpha, t), \tag{8}$$

$$E_{3\alpha} = E_{\alpha 3}, \tag{9}$$

$$E_{33} = \varepsilon_{33}^{(0)}(\zeta^\alpha, t) + \zeta^3 \varepsilon_{33}^{(1)}(\zeta^\alpha, t). \tag{10}$$

## 3. Constitutive Equations

In this work, the FGM constituents are considered to behave as isotropic linear elastic materials. It is worth pointing out that despite this assumption, the FGM analyzed here remains heterogeneous along the thickness direction, and the simple rule of mixtures is used as a homogenization scheme to evaluate the effective material properties of the FGM, which is written as [47,51]

$$P(\zeta^3) = (P_{top} - P_{bot}) V_{top}^i(\zeta^3) + P_{bot}, \tag{11}$$

where  $P(\zeta^3)$  denotes the effective material property (e.g., Young’s modulus, mass density, Poisson’s ratio) along the thickness coordinate,  $P_{top}$  and  $P_{bot}$  are the material properties of the top and bottom constituents, respectively, while  $V_{top}^i(\zeta^3)$  is the volume distribution of the top constituent—through thickness—corresponding to the following forms of the power-law [22]:

$$V_{top}^I(\zeta^3) = \left(\frac{1 + \zeta^3}{2}\right)^n, \tag{12}$$

$$V_{top}^{II}(\xi^3) = \left(\frac{1 - \xi^3}{2}\right)^n, \tag{13}$$

where  $n$  is the volume fraction exponent or power-law index, and its value may be greater or equal to zero. In order to adequately compare with numerical results reported in the literature, the volume distribution  $V_{top}^{II}(\xi^3)$  is also considered in this work.

From now on, to distinguish the aforementioned volume distributions, the volume distribution given by Equation (12) is referred to as FG-I and the volume distribution described by Equation (13) is referred to as FG-II.

Now, for the assumed constituent materials, the fourth-order elasticity tensor, in terms of contravariant vectors, is given by

$$\mathbf{C} = C^{ijkl} \mathbf{g}_i \otimes \mathbf{g}_j \otimes \mathbf{g}_k \otimes \mathbf{g}_l, \tag{14}$$

where the contravariant components are determined by

$$C^{ijkl} = \lambda(\xi^3) g^{ij} g^{kl} + \mu(\xi^3) (g^{ik} g^{jl} + g^{il} g^{jk}). \tag{15}$$

In Equation (15),  $\lambda(\xi^3)$  and  $\mu(\xi^3)$  are the Lamé parameters defined in terms of Young’s modulus,  $E(\xi^3)$ , and Poisson’s ratio,  $\nu(\xi^3)$ , as

$$\lambda(\xi^3) = \frac{\nu(\xi^3) E(\xi^3)}{[1 + \nu(\xi^3)][1 - 2\nu(\xi^3)]}, \quad \mu(\xi^3) = \frac{E(\xi^3)}{2[1 + \nu(\xi^3)]}.$$

Also, in Equation (15),  $g^{ij}$  denotes the contravariant components of the Riemannian metric tensor in the reference configuration, given as  $g^{ij} = \mathbf{g}^i \cdot \mathbf{g}^j$ .

Recalling the considerations of the constituents behavior previously mentioned in this section, the mechanical behavior is assumed to follow Hooke’s law. Then, the relation between the second Piola–Kirchhoff stress tensor and the Green–Lagrange strain tensor is given by

$$\mathbf{S} = \mathbf{C}\mathbf{E}, \tag{16}$$

And the contravariant components of  $\mathbf{S}$  are determined by  $S^{ij} = C^{ijkl} E_{kl}$ .

#### 4. Equations of Motion

The equations of motion associated with the present finite element model are derived using the Hamilton’s principle, which is defined as [52]

$$\int_0^T [\delta K - (\delta U + \delta V)] dt = 0, \tag{17}$$

where  $\delta K$  represents the virtual kinetic energy,  $\delta U$  is the virtual strain energy, and  $\delta V$  is the virtual potential energy due to external loads.

From Hamilton’s principle, the mass matrix, the stiffness matrix, and the load vector can be obtained straightforwardly using the virtual kinetic energy, the virtual strain energy, and the virtual potential energy, respectively. However, for the present study, it is sufficient to compute the stiffness and mass matrices to define the finite element model.

For the displacement field considered here, the virtual kinetic energy is given by

$$\begin{aligned} \delta K = & \int_A \left\{ I_0 (\delta \dot{\mathbf{u}} \cdot \dot{\mathbf{u}}) + I_1 \left[ \frac{h}{2} (\dot{\mathbf{u}} \cdot \delta \dot{\boldsymbol{\varphi}} + \dot{\boldsymbol{\varphi}} \cdot \delta \dot{\mathbf{u}}) \right] + I_2 \left[ \frac{h}{2} (\dot{\mathbf{u}} \cdot \delta \dot{\boldsymbol{\Psi}} \mathbf{n} + \frac{h}{2} \dot{\boldsymbol{\varphi}} \cdot \delta \dot{\boldsymbol{\varphi}} + \dot{\boldsymbol{\Psi}} \mathbf{n} \cdot \delta \dot{\mathbf{u}}) \right] \right. \\ & \left. + I_3 \left[ \frac{h^2}{4} (\dot{\boldsymbol{\varphi}} \cdot \delta \dot{\boldsymbol{\Psi}} \mathbf{n} + \dot{\boldsymbol{\Psi}} \mathbf{n} \cdot \delta \dot{\boldsymbol{\varphi}}) \right] + I_4 \left[ \frac{h^2}{4} (\dot{\boldsymbol{\Psi}} \delta \dot{\boldsymbol{\Psi}} || \mathbf{n} ||^2) \right] \right\} dA, \tag{18} \end{aligned}$$

And the virtual strain energy is given by

$$\delta U = \int_A \left[ A^{ijkl} \delta \varepsilon_{ij}^{(0)} \varepsilon_{kl}^{(0)} + B^{ijkl} \left( \delta \varepsilon_{ij}^{(1)} \varepsilon_{kl}^{(0)} + \delta \varepsilon_{ij}^{(0)} \varepsilon_{kl}^{(1)} \right) + D^{ijkl} \delta \varepsilon_{ij}^{(1)} \varepsilon_{kl}^{(1)} \right] dA. \tag{19}$$

In Equation (18),  $\|\mathbf{n}\|$  is the norm of the normal vector  $\mathbf{n}$ , the dot indicates the partial derivative with respect time, and the mass inertias are defined as

$$\{I_0, I_1, I_2, I_3, I_4\} = \int_{-1}^1 \left\{ 1, \zeta^3, (\zeta^3)^2, (\zeta^3)^3, (\zeta^3)^4 \right\} \rho(\zeta^3) J d\zeta^3,$$

where  $\rho(\zeta^3)$  is the mass density.

In Equation (19), the contravariant components  $A^{ijkl}, B^{ijkl}, D^{ijkl}$  are the effective extensional, extensional–bending coupling, and bending fourth-order stiffness tensor components [47]. Such components are calculated using the following definitions:

$$A^{ijkl} = \int_{-1}^1 C^{ijkl} J d\zeta^3, \quad B^{ijkl} = \int_{-1}^1 \zeta^3 C^{ijkl} J d\zeta^3, \quad D^{ijkl} = \int_{-1}^1 (\zeta^3)^2 C^{ijkl} J d\zeta^3.$$

The expressions of Equations (18) and (19) are used to determine the mass and stiffness matrices, respectively.

### 5. Finite Element Model

The present vibration analysis assumes harmonic motion; therefore, the generalized displacements  $\mathbf{u}(\zeta^\alpha, t), \boldsymbol{\varphi}(\zeta^\alpha, t)$  and the seventh parameter  $\Psi$  can be expressed as [53]

$$\mathbf{u}(\zeta^\alpha, t) = \mathbf{u}(\zeta^\alpha) e^{-i\omega t}, \tag{20}$$

$$\boldsymbol{\varphi}(\zeta^\alpha, t) = \boldsymbol{\varphi}(\zeta^\alpha) e^{-i\omega t}, \tag{21}$$

$$\Psi(\zeta^\alpha, t) = \Psi(\zeta^\alpha) e^{-i\omega t}, \tag{22}$$

Note that  $\omega$  represents the frequency of natural vibration and  $i = \sqrt{-1}$ . For the finite element approximation, the displacements and the seventh parameter are approximated as

$$\mathbf{u}(\zeta^\alpha) = \sum_{j=1}^q \psi_j(\zeta^\alpha) \mathbf{u}, \quad \boldsymbol{\varphi}(\zeta^\alpha) = \sum_{j=1}^q \psi_j(\zeta^\alpha) \boldsymbol{\varphi}, \quad \Psi(\zeta^\alpha) = \sum_{j=1}^q \psi_j(\zeta^\alpha) \Psi. \tag{23}$$

To obtain the mass matrix  $[\mathbf{M}^e]$  and the stiffness matrix  $[\mathbf{K}^e]$  of the element  $e$ , the generalized displacements and the seventh parameter must be replaced by their approximations in the virtual kinetic energy of Equation (18) and in the virtual strain energy of Equation (19), respectively.

Therefore, the finite element model (i.e., the eigenvalue problem) governing the free vibration analysis can be written as

$$([\mathbf{K}] - \omega^2 [\mathbf{M}]) \{\boldsymbol{\Delta}\} = \{0\}, \tag{24}$$

where  $\{\boldsymbol{\Delta}\}$  is the vibration mode vector associated with  $\omega$ , and  $[\mathbf{K}]$  and  $[\mathbf{M}]$  are the global stiffness and mass matrices, respectively, which result from assembling the local stiffness and mass matrices of each element. Note that, if it is the case, boundary conditions must be applied to the global matrices. In this work, the eigenvalue problem is solved using a C++ template library for linear algebra called Eigen [54].

Finally, to illustrate the general process for the present finite element analysis, a flowchart is depicted in Figure 2. The dashed rectangle represents the processes executed for each seven-parameter element in the model mesh.

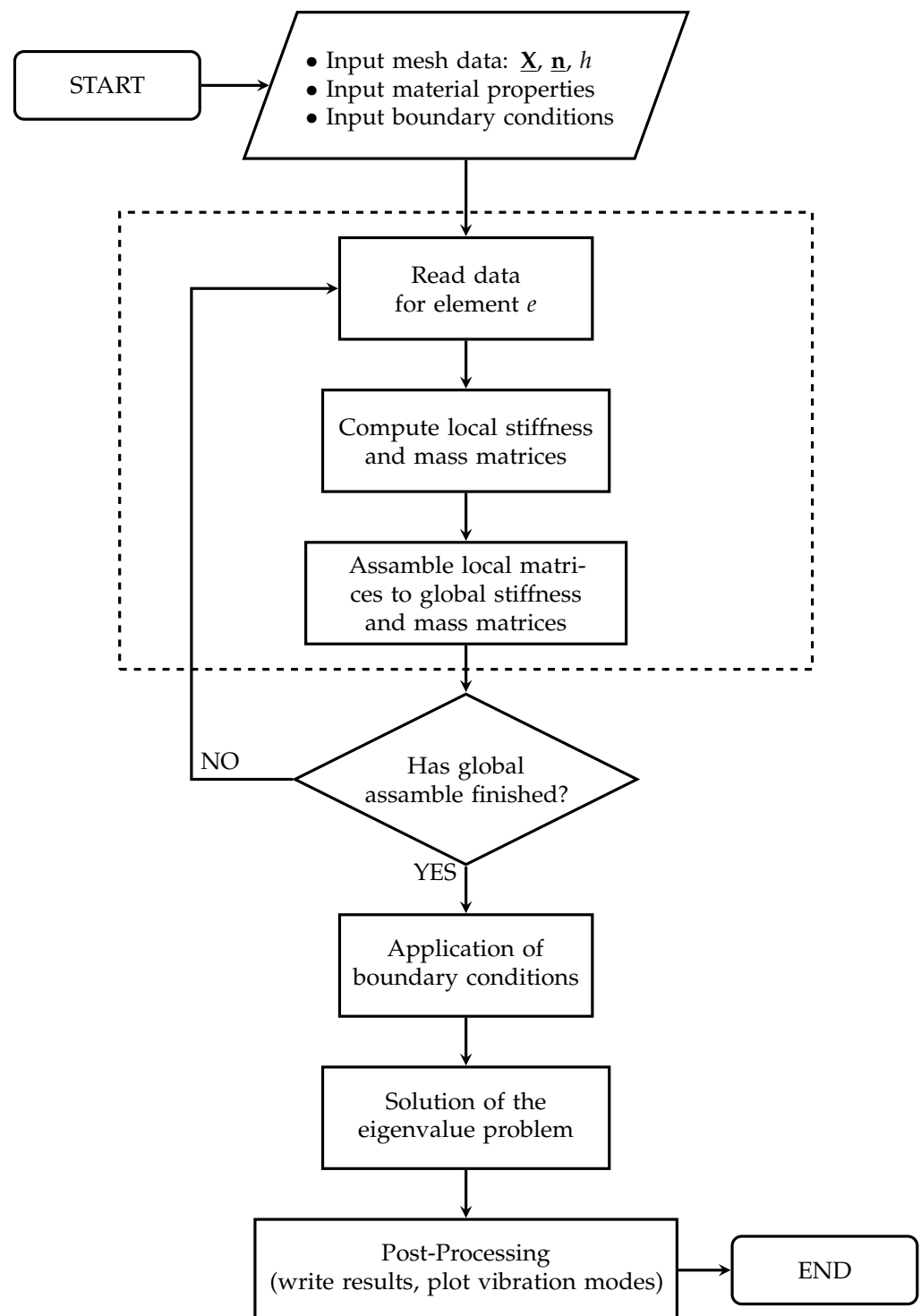


**Figure 2.** Flowchart for the overall finite element analysis process.

## 6. Solid Model

This section presents a brief description about the solid model made in ANSYS, which is used to compare results with the ones obtained by means of the present finite element model.

The solid model is meshed using linear solid elements, i.e., SOLID185 elements. To emulate the mechanical property variations of the FGM, several layers were defined through thickness direction. An isotropic material was assigned to each layer, where its mechanical properties were evaluated according to its position along the thickness direction

and using Equation (11). For instance, in Figure 3, a close-up image of the materials through the thickness direction is depicted.

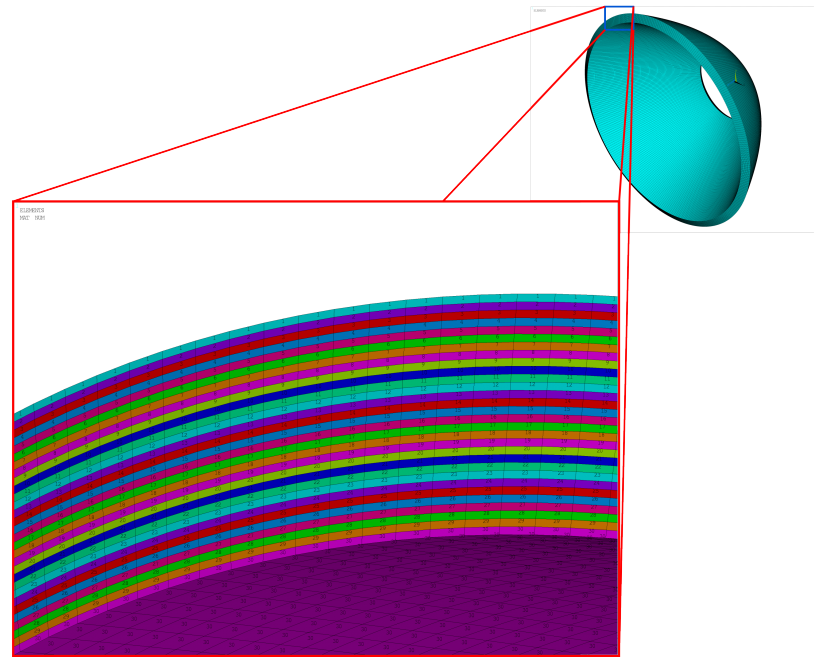


**Figure 3.** Solid model for a parabolic shell and a close-up image showing the materials through thickness direction.

Regarding the boundary conditions used in this study, clamped edge and simply supported edge, these are defined as follows:

- Clamped edge: all the degrees of freedom of the nodes associated with the corresponding edge are constrained.
- Simply supported edge: all the degrees of freedom for the nodes located at the mid-surface of the solid model are constrained, and the remaining nodes are constrained in the tangential and the thickness directions.

Note that, in order to obtain nodes at the mid-surface, an even number of layers must be defined, since linear solid elements are used.

## 7. Results

In this section, the geometrical parameters of the shell structures analyzed here are introduced. In addition, the convergence studies and numerical comparisons are included. At the end, the influence of the geometrical parameters and material properties on the natural frequencies is presented to illustrate the performance of the present model. All natural frequencies are reported in Hertz.

### 7.1. Geometrical Parameters

For the shells studied here, the position vector used to describe the mid-surface of the shell and the functions for variation of the thickness are listed below. In addition, the geometrical parameters are depicted in Figures 4–6. Note that the thickness variation is linear for all the shells, and the conical, parabolic, and hemispherical shells are truncated.



1. Conical shell

- Mid-surface:

$$\mathbf{r}(\theta, z) = r(z) \cos \theta \hat{\mathbf{i}} + r(z) \sin \theta \hat{\mathbf{j}} + z \hat{\mathbf{k}}, \quad \begin{matrix} 0 \leq z \leq L \cos \alpha \\ 0 \leq \alpha < \pi/2 \\ 0 \leq \theta \leq 2\pi \end{matrix} \quad (25)$$

where  $r(z) = r_0 + \frac{r_1 - r_0}{L \cos \alpha} z$ .

- Thickness variation:

$$h(z) = h_0 + (h_1 - h_0) \frac{z}{L \cos \alpha}, \quad \begin{matrix} 0 \leq z \leq L \cos \alpha \\ 0 \leq \alpha < \pi/2 \end{matrix} \quad (26)$$

2. Cylindrical shell ( $\alpha = 0$ )

- Mid-surface:

$$\mathbf{r}(\theta, z) = r_0 \cos \theta \hat{\mathbf{i}} + r_0 \sin \theta \hat{\mathbf{j}} + z \hat{\mathbf{k}}, \quad \begin{matrix} 0 \leq z \leq L \\ 0 \leq \theta \leq 2\pi \end{matrix} \quad (27)$$

- Thickness variation:

$$h(z) = h_0 \left[ 1 + \frac{h_1 - h_0}{h_0} \frac{z}{L} \right], \quad 0 \leq z \leq L \quad (28)$$

3. Parabolic shell

- Mid-surface:

$$\mathbf{r}(\varphi, \theta) = r(\varphi) \cos \theta \hat{\mathbf{i}} + r(\varphi) \sin \theta \hat{\mathbf{j}} + \frac{r(\varphi)^2}{4F} \hat{\mathbf{k}}, \quad \begin{matrix} \varphi_0 \leq \varphi \leq \varphi_1 \\ 0 \leq \theta \leq 2\pi \end{matrix} \quad (29)$$

where  $r(\varphi) = 2F \tan \varphi$ , with  $F$  being the focal distance [55].

- Thickness variation:

$$h(\varphi) = h_0 \left[ 1 + \beta \left( \frac{\varphi - \varphi_0}{\varphi_1 - \varphi_0} \right) \right], \quad \varphi_0 \leq \varphi \leq \varphi_1 \quad (30)$$

4. Hemispherical shell

- Mid-surface:

$$\mathbf{r}(\varphi, \theta) = r_0 \sin \varphi \cos \theta \hat{\mathbf{i}} + r_0 \sin \varphi \sin \theta \hat{\mathbf{j}} + r_0 \cos \varphi \hat{\mathbf{k}}, \quad \begin{matrix} \varphi_0 \leq \varphi \leq \varphi_1 \\ 0 \leq \theta \leq 2\pi \end{matrix} \quad (31)$$

- Thickness variation:

$$h(\varphi) = h_0 \left[ 1 - \beta \left( \frac{\varphi - \varphi_0}{\varphi_1 - \varphi_0} \right) \right], \quad \varphi_0 \geq \varphi \geq \varphi_1 \quad (32)$$

An additional parameter, used in the following sections when reporting natural frequencies of shells with variable thickness, is the average thickness,  $h_m$ , which is defined as

$$h_m = \frac{h_0 + h_1}{2}. \quad (33)$$

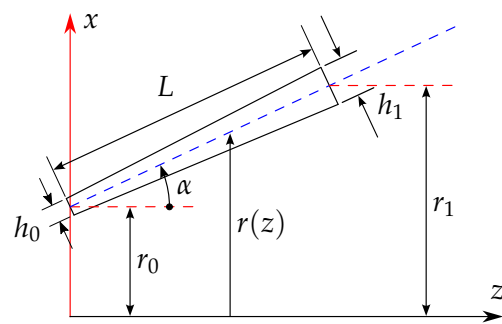


Figure 4. Geometrical parameters and revolution profile for a conical shell.

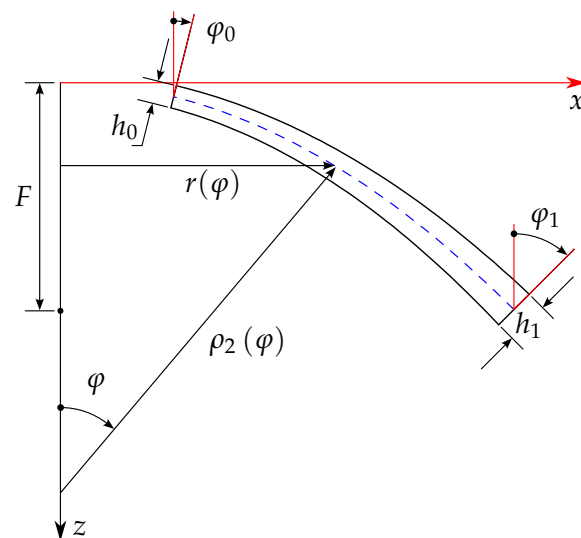


Figure 5. Geometrical parameters and revolution profile for a parabolic shell.

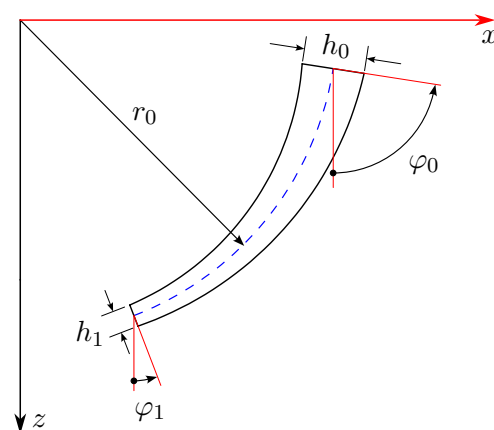


Figure 6. Geometrical parameters and revolution profile for a hemispherical shell.

### 7.2. Boundary Conditions

For convenience, a nomenclature based on capital letters is used to describe the boundary conditions applied in each case of study. The letters C, F, and S denote a clamped edge, a free edge, and a simply supported edge, respectively.

The clamped edge (C) restricts all the degrees of freedom associated with the nodes at the end that represent the maximum thickness, while the nodes located at a free edge (F) are unrestricted.

Furthermore, the parabolic shell structure analyzed here is subjected to SF boundary conditions (i.e., simply-supported-free). Therefore, the degrees of freedom of the nodes at the simply supported edge (S) are restricted as follows:

$$\mathbf{u} = \Psi = 0. \tag{34}$$

### 7.3. Material Properties

The mechanical properties used in this work, for the bottom and top constituents, are listed below [23]:

- Aluminum:  $E_{bot} = 70$  GPa,  $\rho_{bot} = 2707$  kg/m<sup>3</sup>,  $\nu_{bot} = 0.3$ ;
- Zirconia:  $E_{top} = 168$  GPa,  $\rho_{top} = 5700$  kg/m<sup>3</sup>,  $\nu_{top} = 0.3$ .

where  $E_i$  is the modulus of elasticity,  $\rho_i$  denotes the mass density, and  $\nu_i$  the Poisson’s ratio. Note that subindex  $i$  indicates the surface position.

### 7.4. Convergence Study

To achieve mesh independence, convergence studies were performed for each shell geometry analyzed in this work. The results of these studies are presented and discussed in Appendix A. It is worth mentioning that for all cases analyzed with the present finite element model, seven-parameter elements of order  $p = 8$  were used to mesh the domains.

In general, for the shells with uniform thickness (UT) and linear variable thickness (LVT) studied in this work, it is observed that convergence is obtained with a mesh size of 25 elements—within the first ten frequencies. The only case where a good convergence is achieved with a mesh size of 16 elements is the parabolic shell with UT.

### 7.5. Numerical Verification

To verify the performance of the present model, the natural frequencies obtained were compared with those results reported in the literature. It must be noted that the numerical comparisons correspond to shells with uniform thickness. In addition, a comparison is included with results obtained by using linear solid elements (SOLID185). The latter allows us to verify the behavior of the present model for shells with thickness variation.

In the following comparisons, the natural frequencies obtained by means of the present model are indicated by the label 7-PL. On the other hand, the label 3D represents the results obtained using solid elements in the commercial code ANSYS.

Tables 1–3 present a comparison for conical, cylindrical, and parabolic shells, respectively. The natural frequencies obtained using the present formulation show very good agreement with the ones reported in the literature and the ones computed by means of solid elements in ANSYS.

**Table 1.** Comparison for a conical shell with UT and CF boundary conditions (FG-II).

$n$	Model	Natural Frequency							
		$f_1-f_2$	$f_3-f_4$	$f_5-f_6$	$f_7-f_8$	$f_9-f_{10}$	$f_{11}-f_{12}$	$f_{13}-f_{14}$	$f_{15}$
0.6	7-PL	206.20	225.98	279.08	318.23	348.99	355.98	398.53	444.36
	3D *	205.93	226.02	279.55	318.32	348.57	356.80	397.36	444.55
	FSDT [22]	205.96	225.52	277.93	318.18	349.48	-	-	-
1	7-PL	205.12	224.88	277.82	316.39	347.13	354.42	396.71	441.88
	3D *	204.79	224.81	278.08	316.47	346.59	354.94	395.26	442.02
	FSDT [22]	204.91	224.44	276.66	316.32	347.66	-	-	-
5	7-PL	204.19	228.16	285.59	309.64	346.64	366.47	404.55	434.38
	3D *	203.69	227.75	285.14	309.65	345.64	365.74	402.10	434.30
	FSDT [22]	203.93	227.67	284.26	309.57	347.08	-	-	-

\* 1,188,000 SOLID185 elements.

**Table 2.** Comparison for a cylindrical shell with UT and CF boundary conditions (FG-II).

<i>n</i>	Model	Natural Frequency							
		$f_1-f_2$	$f_3-f_4$	$f_5-f_6$	$f_7-f_8$	$f_9$	$f_{10}-f_{11}$	$f_{12}-f_{13}$	$f_{14}-f_{15}$
0.6	7-PL	148.95	213.76	250.23	375.14	414.34	418.82	454.43	523.52
	3D *	148.68	212.79	250.17	372.70	414.69	417.01	453.73	519.60
	FSDT [22]	150.03	212.94	250.74	370.63	415.47	420.39	-	-
1	7-PL	148.07	213.04	248.56	374.04	411.54	416.78	451.68	521.55
	3D *	147.74	211.83	248.49	371.09	411.89	414.67	450.87	517.02
	FSDT [22]	149.29	212.22	249.31	369.46	412.97	418.46	-	-
5	7-PL	147.51	220.44	242.75	388.72	401.19	422.08	446.11	537.48
	3D *	147.04	218.65	242.64	384.31	401.56	418.91	444.89	530.75
	FSDT [22]	148.75	219.49	243.43	383.71	402.56	423.57	-	-

\* 990,000 SOLID185 elements.

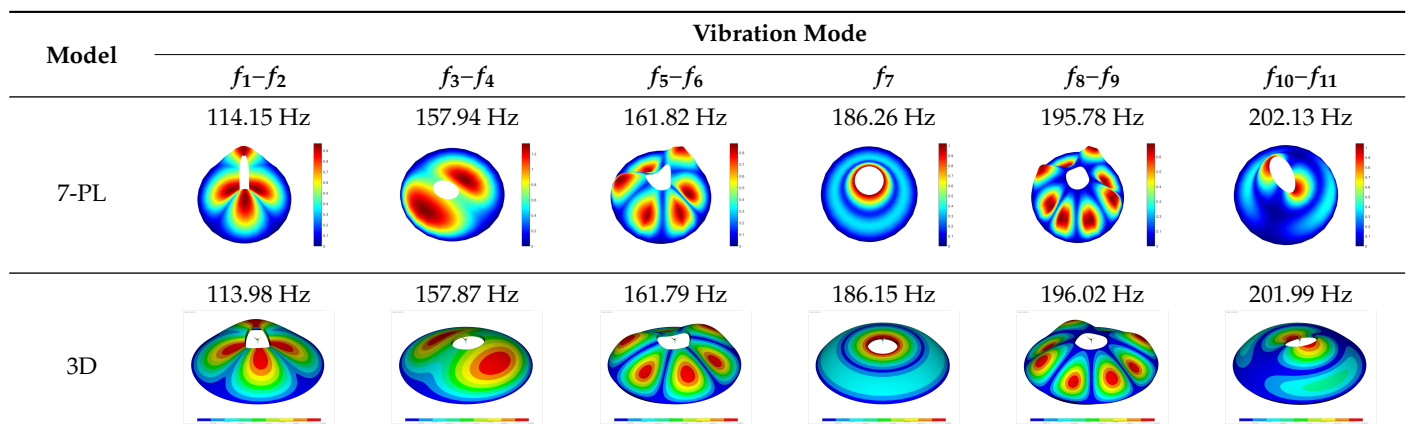
**Table 3.** Comparison for a parabolic shell with UT and SF boundary conditions (FG-I).

<i>n</i>	Model	Natural Frequency							
		$f_1-f_2$	$f_3-f_4$	$f_5-f_6$	$f_7$	$f_8$	$f_9$	$f_{10}-f_{11}$	$f_{12}-f_{13}$
0.6	7-PL	115.04	162.58	162.67	190.60	194.75	194.75	205.35	218.29
	3D *	115.01	162.54	162.88	190.60	195.42	195.42	205.37	217.36
	FSDT [23]	115.40	162.85	165.07	193.28	193.28	196.66	210.82	-
1	7-PL	114.15	161.55	161.83	189.18	193.88	193.88	203.94	217.37
	3D *	114.10	161.52	161.98	189.16	194.43	194.43	203.95	216.39
	FSDT [23]	114.49	161.95	164.01	192.32	192.32	195.22	209.38	-
5	7-PL	114.15	157.94	161.82	186.26	195.78	195.78	202.13	218.63
	3D *	113.98	157.87	161.79	186.15	196.02	196.02	201.99	217.16
	FSDT [23]	114.44	160.33	161.78	194.04	194.04	194.05	207.19	-

\* 840,000 SOLID185 elements.

In addition, Table 4 shows a comparison of the vibration modes for a parabolic shell with uniform thickness and with a volume distribution of the type FG-I. A very good coincidence is observed in the depicted modes. Moreover, similar modes were reported in [23].

**Table 4.** Vibration mode comparison for a parabolic shell with UT and SF boundary conditions, *n* = 5 (FG-I).



Finally, a comparison of the natural frequencies for a hemispherical shell with constant thickness and CF boundary conditions is shown in Table 5. The results of the present model and the 3D model are in accordance with those reported in [23].

**Table 5.** Comparison for a hemispherical shell with UT and CF boundary conditions (FG-I).

<i>n</i>	Model	Natural Frequency							
		$f_1-f_2$	$f_3-f_4$	$f_5-f_6$	$f_7-f_8$	$f_9$	$f_{10}-f_{11}$	$f_{12}-f_{13}$	$f_{14}-f_{15}$
0.6	7-PL	142.75	204.61	286.86	335.28	379.76	411.97	450.15	457.29
	3D *	143.01	205.53	286.90	336.75	379.75	411.97	450.15	459.24
	FSDT [23]	142.56	204.01	286.77	334.14	379.53	411.83	-	-
1	7-PL	141.76	203.20	284.87	332.97	377.05	409.05	446.97	454.12
	3D *	142.01	204.09	284.89	334.38	377.04	409.05	446.96	456.00
	FSDT [23]	141.59	202.64	284.78	331.87	376.84	408.93	-	-
5	7-PL	141.34	207.57	278.77	338.35	369.92	401.34	440.98	456.69
	3D *	141.43	207.98	278.72	338.95	369.76	401.19	440.70	457.67
	FSDT [23]	141.14	206.90	278.68	337.12	369.68	401.19	-	-

\* 1,017,000 SOLID185 elements.

7.6. Numerical Results

The main aim of this section is to present the natural frequencies for several type of shells with LVT, such as conical, cylindrical, parabolic, and hemispherical. Along with the present results (7-PL), the natural frequencies obtained by means of solid elements in ANSYS are included for comparison purposes. For all study cases and listed frequencies, the maximum relative errors of the present model with respect to 3D result are reported for each power-law index.

The natural frequencies for conical shells with LVT under CF boundary conditions are presented in Tables 6–8 for different values of the ratio  $r_0/h_m$  and angle  $\alpha$ . The volume distribution of the top constituent follows the expression of Equation (13), i.e., FG-II.

**Table 6.** Natural frequencies for conical shells with LVT and CF boundary conditions (FG-II,  $r_0/h_m = 2.5, h_m = 3/4, L/h_m = 10, h_1/h_0 = 2$ ).

	$\alpha = 30^\circ$						$\alpha = 60^\circ$					
	<i>n</i>		<i>n</i>		<i>n</i>		<i>n</i>		<i>n</i>		<i>n</i>	
	0.6	1	5	0.6	1	5	0.6	1	5	0.6	1	5
	7PL	3D	7PL	3D	7PL	3D	7PL	3D	7PL	3D	7PL	3D
$f_1-f_2$	101.96	99.10	101.58	98.62	103.00	99.57	88.96	86.55	88.61	86.12	90.34	87.46
$f_3-f_4$	125.12	124.75	124.38	124.02	121.97	121.50	93.71	92.40	93.41	91.98	92.86	91.27
$f_5$	160.29	155.02	159.92	154.34	164.31	157.48	106.33	105.18	106.04	104.73	104.82	103.43
$f_6$	160.29	155.02	159.92	154.34	164.31	157.48	120.96	117.73	120.49	117.11	124.14	119.97
$f_7$	181.57	177.36	180.78	176.37	182.29	176.86	120.96	117.73	120.49	117.11	124.14	119.97
$f_8$	181.57	177.36	180.78	176.37	182.29	176.86	154.15	151.57	153.71	150.91	153.15	149.78
$f_9$	205.72	204.42	204.22	203.21	198.99	199.79	159.58	156.52	159.04	155.78	159.71	155.72
$f_{10}$	205.91	204.42	204.77	203.21	201.79	199.86	159.58	156.52	159.04	155.78	159.71	155.72
$f_{11}$	205.91	206.41	204.77	205.02	201.79	199.87	164.50	160.34	163.86	159.44	168.87	163.06
$f_{12}$	207.73	206.85	207.01	205.99	202.72	201.65	164.50	160.34	163.86	159.44	168.87	163.06
Max. Error	3.40%	-	3.61%	-	4.34%	-	2.77%	-	2.89%	-	3.56%	-

**Table 7.** Natural frequencies for conical shells with LVT and CF boundary conditions (FG-II,  $r_0/h_m = 5, h_m = 3/4, L/h_m = 10, h_1/h_0 = 2$ ).

	$\alpha = 30^\circ$						$\alpha = 60^\circ$					
	0.6		1		5		0.6		1		5	
	7PL	3D	7PL	3D	7PL	3D	7PL	3D	7PL	3D	7PL	3D
$f_1-f_2$	73.76	72.43	73.38	72.01	73.23	71.65	64.23	62.47	63.98	62.16	64.69	62.64
$f_3-f_4$	84.73	82.08	84.41	81.68	86.67	83.55	72.78	71.76	72.55	71.44	71.84	70.62
$f_5-f_6$	104.14	103.72	103.58	103.14	101.67	101.15	77.18	74.79	76.86	74.40	79.19	76.38
$f_7$	124.04	120.57	123.65	120.00	127.76	123.35	82.39	81.54	82.17	81.20	80.96	79.93
$f_8$	124.04	120.57	123.65	120.00	127.76	123.35	105.15	102.48	104.71	101.93	108.29	104.89
$f_9$	151.23	147.91	150.50	147.07	149.20	147.02	105.15	102.48	104.71	101.93	108.29	104.89
$f_{10}$	151.23	147.91	150.50	147.07	151.13	147.02	119.33	115.18	118.91	114.62	119.88	114.99
$f_{11}$	152.28	151.27	151.73	150.61	151.13	148.02	121.86	117.67	121.40	117.08	122.83	117.87
$f_{12}$	156.70	152.27	156.02	151.42	158.92	153.33	121.86	117.67	121.40	117.08	122.83	117.87
Max. Error	3.22%	-	3.34%	-	3.74%	-	3.61%	-	3.74%	-	4.25%	-

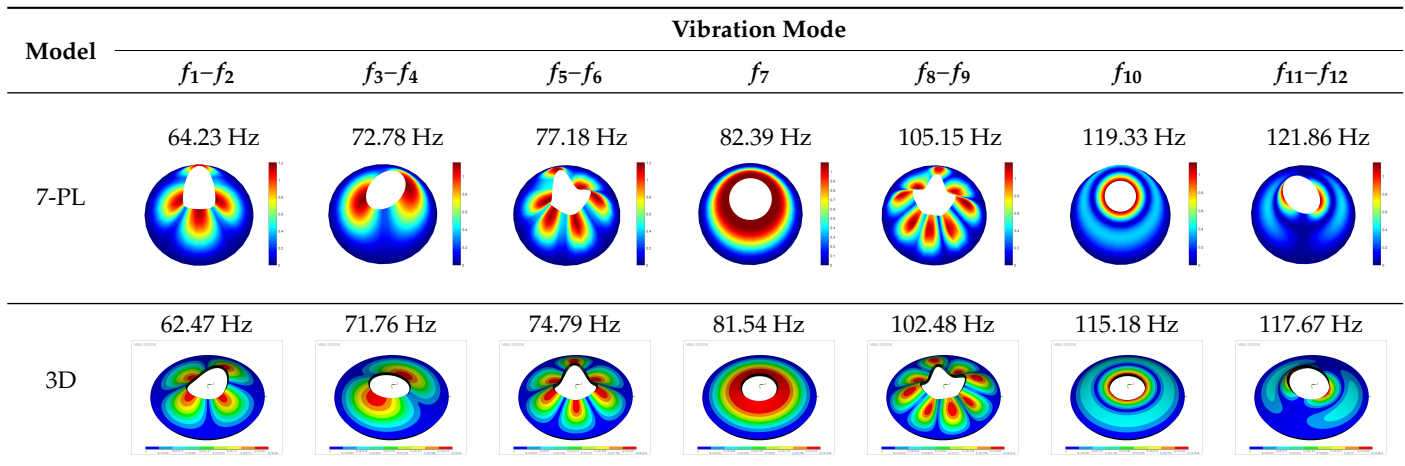
**Table 8.** Natural frequencies for conical shells with LVT and CF boundary conditions (FG-II,  $r_0/h_m = 10, h_m = 3/4, L/h_m = 10, h_1/h_0 = 2$ ).

	$\alpha = 30^\circ$						$\alpha = 60^\circ$					
	0.6		1		5		0.6		1		5	
	7PL	3D	7PL	3D	7PL	3D	7PL	3D	7PL	3D	7PL	3D
$f_1-f_2$	52.69	51.04	52.43	50.75	52.89	51.00	45.53	43.84	45.36	43.63	45.57	43.66
$f_3-f_4$	58.04	55.90	57.78	55.60	58.52	56.87	46.64	44.56	46.44	44.33	47.45	45.13
$f_5-f_6$	59.39	58.42	59.08	58.08	59.31	57.38	50.32	48.99	50.15	48.77	49.73	48.21
$f_7$	72.78	70.51	72.48	70.14	74.97	72.28	54.03	52.76	53.87	52.48	53.19	51.78
$f_8$	72.78	70.51	72.48	70.14	74.98	72.28	54.96	52.76	54.71	52.48	56.50	54.00
$f_9$	77.08	76.52	76.69	76.11	75.30	74.63	54.96	52.81	54.71	52.58	56.50	54.00
$f_{10}$	77.08	76.52	76.69	76.11	75.30	74.63	68.97	66.86	68.65	66.49	71.16	68.65
$f_{11}$	92.91	91.54	92.51	91.07	90.61	89.98	68.97	66.86	68.65	66.49	71.16	68.65
$f_{12}$	93.83	91.54	93.45	91.07	96.85	93.97	87.13	85.17	86.73	84.70	89.95	87.44
Max. Error	3.84%	-	3.92%	-	3.73%	-	4.66%	-	4.76%	-	5.14%	-

From the comparisons presented in Tables 6–8, the maximum values of relative error ranges from 3.22% to 4.34% for conical shells with an angle  $\alpha = 30^\circ$ , and the maximum value is obtained when  $n = 5$ . Regarding the conical shells with  $\alpha = 60^\circ$ , the maximum errors are found in a range from 2.77% to 5.14%, with the maximum value occurring when  $n = 5$ . Considering fixed values of the power-law exponent, the natural frequencies decrease as the value of ratio  $r_0/h_m$  increases, which is an expected behavior since the ratio values reported are related to thick and thin shells. In addition, the angle  $\alpha$  also has an influence on the natural frequencies as it can be seen for fixed ratios of  $r_0/h_m$ , that is, lower values are obtained as the angle  $\alpha$  increases.

In Table 9, several vibration modes for a conical shell with LVT, CF boundary conditions, and  $n = 0.6$  are compared with those obtained by means of the solid elements (3D model). For both models, the vibration modes are very similar.

**Table 9.** Vibration modes for a conical shell with LVT, CF boundary conditions and  $\alpha = 60^\circ$ ,  $n = 0.6$  (FG-II,  $r_0/h_m = 5$ ,  $h_m = 3/4$ ,  $L/h_m = 10$ ,  $h_1/h_0 = 2$ ).



In Tables 10–12, the natural frequencies for several ratios  $r_0/h_m$  of a cylindrical shell with LVT subjected to CF boundary conditions are reported.

**Table 10.** Natural frequencies for a cylindrical shell with LVT and CF boundary conditions (FG-II,  $r_0/h_m = 2.5$ ,  $h_m = 3/4$ ,  $L/h_m = 10$ ,  $h_1/h_0 = 2$ ).

	<i>n</i>					
	0.6		1		5	
	7PL	3D	7PL	3D	7PL	3D
$f_1-f_2$	64.07	63.72	63.28	62.98	62.17	61.75
$f_3$	123.97	121.23	122.50	120.98	119.37	121.87
$f_4$	129.65	121.23	129.78	120.98	134.06	124.17
$f_5$	129.65	126.14	129.78	124.89	134.06	124.17
$f_6-f_7$	191.89	191.01	190.34	189.49	186.81	185.65
$f_8$	203.99	203.77	202.46	202.23	197.49	197.18
$f_9-f_{10}$	217.19	204.85	217.00	204.04	220.95	205.82
$f_{11}$	313.85	294.01	314.23	293.37	320.46	299.19
$f_{12}$	313.85	294.01	314.23	293.37	323.41	299.19
Max. Error	6.95%	-	7.28%	-	8.10%	-

**Table 11.** Natural frequencies for a cylindrical shell with LVT and CF boundary conditions (FG-II,  $r_0/h_m = 5$ ,  $h_m = 3/4$ ,  $L/h_m = 10$ ,  $h_1/h_0 = 2$ ).

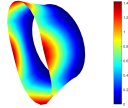
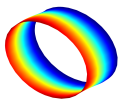
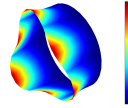
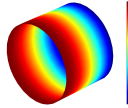
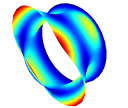
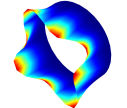
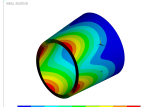
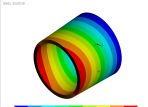
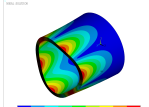
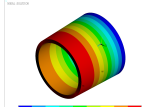
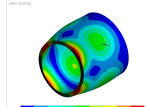
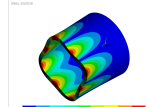
	<i>n</i>					
	0.6		1		5	
	7PL	3D	7PL	3D	7PL	3D
$f_1-f_2$	58.50	56.58	58.17	56.21	58.80	56.58
$f_3-f_4$	79.10	78.91	78.44	78.29	76.87	76.63
$f_5-f_6$	96.15	92.18	95.92	91.81	99.21	94.57
$f_7$	125.24	125.97	124.11	124.94	120.98	121.83
$f_8-f_9$	157.38	153.83	156.55	152.89	156.72	152.33
$f_{10}-f_{11}$	162.94	156.82	162.61	156.20	168.25	160.75
$f_{12}-f_{13}$	179.49	173.24	178.90	172.36	182.66	174.78
Max. Error	4.31%	-	4.48%	-	4.91%	-

**Table 12.** Natural frequencies for a cylindrical shell with LVT and CF boundary conditions (FG-II,  $r_0/h_m = 10, h_m = 3/4, L/h_m = 10, h_1/h_0 = 2$ ).

	<i>n</i>					
	0.6		1		5	
	7PL	3D	7PL	3D	7PL	3D
$f_1-f_2$	48.37	46.58	48.11	46.30	48.72	46.67
$f_3-f_4$	54.00	53.11	53.65	52.75	53.14	52.09
$f_5-f_6$	58.00	55.57	57.75	55.28	59.51	56.76
$f_7-f_8$	76.64	75.27	76.13	74.90	74.61	74.25
$f_9-f_{10}$	78.00	76.34	77.70	75.84	80.52	77.33
$f_{11}-f_{12}$	104.59	101.58	104.20	101.09	108.05	104.37
Max. Error	4.36%	-	4.46%	-	4.84%	-

For the natural frequencies presented in Tables 10–12, corresponding to cylindrical shells, the range for the maximum errors is between 4.31% and 8.10%, with the maximum value occurring in the case when  $r_0/h_m = 2.5$  and  $n = 5$ . Note that the aforementioned radius-to-thickness ratio describes a very thick shell. However, for greater values of the ratio, the value of errors are below 4.91%. For illustration purposes, a comparison of several vibration modes of a cylindrical shell with LVT, CF boundary conditions, and  $n = 5$  is presented in Table 13.

**Table 13.** Vibration modes for a cylindrical shell with LVT and CF boundary conditions,  $n = 5$  (FG-II,  $r_0/h_m = 5, h_m = 3/4, L/h_m = 10, h_1/h_0 = 2$ ).

Model	Vibration Mode					
	$f_1-f_2$	$f_3-f_4$	$f_5-f_6$	$f_7$	$f_8-f_9$	$f_{10}$
	58.80 Hz	76.87 Hz	99.21 Hz	120.98 Hz	156.72 Hz	168.25 Hz
7-PL						
	56.58 Hz	76.63 Hz	94.57 Hz	121.83 Hz	152.33 Hz	160.75 Hz
3D						

Natural frequencies for parabolic shells with LVT and under SF boundary conditions are presented in Tables 14–16. The volume distribution of the top constituent follows the expression of Equation (12), i.e., FG-I.

From the comparisons presented for parabolic shells in Tables 14–16, the maximum values of relative error are within the range of 3.18% to 4.59%. In these comparisons, note that for a thin shell (e.g.,  $F/h_m = 20$ ), the maximum error occurs when  $n = 0.6$ , conversely to minor values of the ratio. For a fixed value of the volume fraction exponent, a decrease in values of the natural frequencies is observed as the ratio  $F/h_m$  increases.



**Table 14.** Natural frequencies for a parabolic shell with LVT and SF boundary conditions (FG-I,  $F/h_m = 5, F = 0.875 \text{ m}, \beta = 1.5, \varphi_0 = \pi/6, \varphi_1 = \pi/3$ ).

	<i>n</i>					
	0.6		1		5	
	7PL	3D	7PL	3D	7PL	3D
$f_1-f_2$	138.98	133.61	137.35	132.00	136.85	130.85
$f_3-f_4$	181.80	177.58	180.53	176.21	183.46	179.06
$f_5-f_6$	232.68	232.88	230.73	230.96	225.53	225.64
$f_7-f_8$	252.57	252.06	251.06	250.34	255.86	254.68
$f_9-f_{10}$	302.11	298.29	300.57	296.72	299.31	294.62
$f_{11}-f_{12}$	306.54	300.91	305.01	299.20	309.83	303.04
Max. Error	4.02%	-	4.05%	-	4.59%	-

**Table 15.** Natural frequencies for a parabolic shell with LVT and SF boundary conditions (FG-I,  $F/h_m = 10, F = 0.875 \text{ m}, \beta = 1.5, \varphi_0 = \pi/6, \varphi_1 = \pi/3$ ).

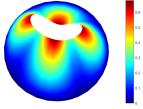
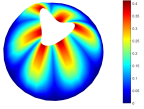
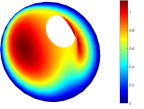
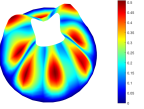
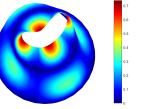
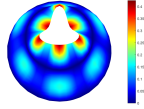
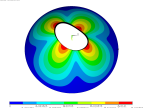
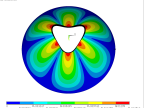
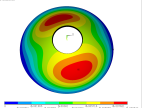
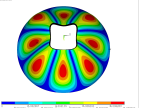
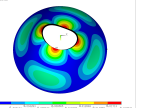
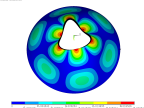
	<i>n</i>					
	0.6		1		5	
	7PL	3D	7PL	3D	7PL	3D
$f_1-f_2$	119.48	115.77	118.64	114.89	118.94	116.41
$f_3-f_4$	122.05	119.91	120.77	118.66	120.81	116.84
$f_5-f_6$	172.76	172.33	171.76	171.22	173.29	172.75
$f_7-f_8$	208.23	210.71	207.04	209.37	209.48	211.53
$f_9-f_{10}$	228.63	227.59	227.39	226.31	223.38	223.67
$f_{11}-f_{12}$	230.51	230.82	228.80	229.13	225.88	224.48
Max. Error	3.21%	-	3.26%	-	3.40%	-

**Table 16.** Natural frequencies for a parabolic shell with LVT and SF boundary conditions (FG-I,  $F/h_m = 20, F = 0.875 \text{ m}, \beta = 1.5, \varphi_0 = \pi/6, \varphi_1 = \pi/3$ ).

	<i>n</i>					
	0.6		1		5	
	7PL	3D	7PL	3D	7PL	3D
$f_1-f_2$	78.31	78.03	77.70	77.41	78.79	78.05
$f_3-f_4$	112.95	114.96	112.32	114.26	112.91	112.39
$f_5-f_6$	116.41	116.08	115.36	115.04	115.13	116.39
$f_7-f_8$	155.52	159.99	154.62	158.99	154.93	158.71
$f_9-f_{10}$	170.88	176.93	169.87	175.80	170.10	175.69
$f_{11}-f_{12}$	182.82	184.09	181.73	182.96	179.73	180.76
Max. Error	3.42%	-	3.38%	-	3.18%	-

To complement the comparisons presented for parabolic shells, the vibration modes corresponding to a parabolic shell with LVT, SF boundary conditions, and  $n = 0.6$  are shown in Table 17. It can be noted that similar contours are obtained using both models.

**Table 17.** Vibration modes for a parabolic shell with LVT and SF boundary conditions,  $n = 0.6$  (FG-I,  $F/h_m = 5, F = 0.875 \text{ m}, \beta = 1.5, \varphi_0 = \pi/6, \varphi_1 = \pi/3$ ).

Model	Vibration Mode					
	$f_1-f_2$	$f_3-f_4$	$f_5-f_6$	$f_7-f_8$	$f_9-f_{10}$	$f_{11}-f_{12}$
7-PL	138.98 Hz 	181.80 Hz 	232.68 Hz 	252.57 Hz 	302.11 Hz 	306.54 Hz 
3D	133.61 Hz 	177.58 Hz 	232.88 Hz 	252.06 Hz 	298.29 Hz 	300.91 Hz 

For the hemispherical shell, the natural frequencies for several values of the ratio  $r_0/h_m$  are presented in Tables 18–21.

**Table 18.** Natural frequencies for a hemispherical shell with LVT and CF boundary conditions (FG-I,  $r_0/h_m = 2.5, r_0 = 2 \text{ m}, \beta = 2, \varphi_0 = \pi/2, \varphi_1 = \pi/6$ ).

	$n$					
	0.6		1		5	
	7PL	3D	7PL	3D	7PL	3D
$f_1-f_2$	442.59	423.35	437.86	418.65	434.18	413.44
$f_3-f_4$	458.16	425.35	453.14	420.03	456.14	419.90
$f_5$	619.59	598.02	615.52	589.93	598.59	583.48
$f_6$	634.79	626.47	625.45	621.43	620.69	605.34
$f_7-f_8$	687.08	643.50	679.83	635.00	683.42	632.22
$f_9$	756.26	718.08	747.01	708.77	738.23	693.93
$f_{10}-f_{11}$	774.88	721.68	763.24	711.05	757.58	699.82
$f_{12}$	906.26	881.70	899.18	868.81	874.43	854.77
Max. Error	7.16%	-	7.31%	-	7.95%	-

**Table 19.** Natural frequencies for a hemispherical shell with LVT and CF boundary conditions (FG-I,  $r_0/h_m = 5, r_0 = 2 \text{ m}, \beta = 2, \varphi_0 = \pi/2, \varphi_1 = \pi/6$ ).

	$n$					
	0.6		1		5	
	7PL	3D	7PL	3D	7PL	3D
$f_1-f_2$	312.90	292.48	310.07	289.79	315.58	293.36
$f_3-f_4$	382.61	375.14	379.14	371.83	375.03	366.38
$f_5-f_6$	461.50	433.85	457.54	429.81	467.90	437.24
$f_7$	563.95	542.00	556.87	536.10	550.30	528.42
$f_8$	632.93	598.01	625.57	591.51	619.64	588.23
$f_9$	632.93	598.02	625.57	591.51	626.45	588.23
$f_{10}$	634.47	614.37	628.57	608.52	626.45	602.37
$f_{11}$	639.65	642.00	635.46	637.34	626.63	621.72
$f_{12}$	687.48	654.55	681.40	648.09	694.55	655.38
Max. Error	6.53%	-	6.54%	-	7.04%	-

**Table 20.** Natural frequencies for a hemispherical shell with LVT and CF boundary conditions (FG-I,  $r_0/h_m = 10, r_0 = 2 \text{ m}, \beta = 2, \varphi_0 = \pi/2, \varphi_1 = \pi/6$ ).

	<i>n</i>					
	0.6		1		5	
	7PL	3D	7PL	3D	7PL	3D
$f_1-f_2$	213.69	204.60	212.06	203.05	213.72	203.73
$f_3-f_4$	278.82	261.85	276.89	259.97	284.29	266.47
$f_5-f_6$	348.85	347.55	346.21	344.94	340.23	338.50
$f_7-f_8$	428.30	410.50	425.27	407.47	435.41	416.22
$f_9$	478.89	465.83	474.40	461.85	471.54	457.11
$f_{10}-f_{11}$	496.81	482.31	492.13	478.18	490.25	474.15
$f_{12}$	541.01	522.79	536.21	518.42	538.24	517.91
Max. Error	6.08%	-	6.11%	-	6.27%	-

**Table 21.** Natural frequencies for a hemispherical shell with LVT and CF boundary conditions (FG-I,  $r_0/h_m = 20, r_0 = 2 \text{ m}, \beta = 2, \varphi_0 = \pi/2, \varphi_1 = \pi/6$ ).

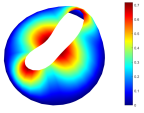
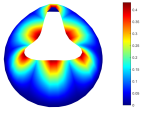
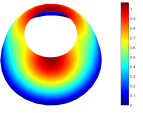
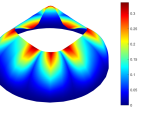
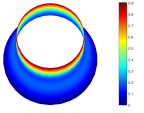
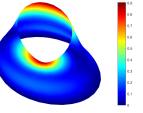
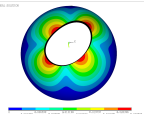
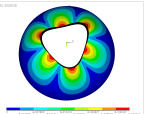
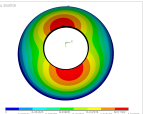
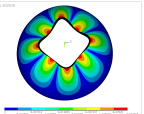
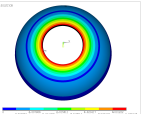
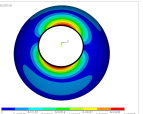
	<i>n</i>					
	0.6		1		5	
	7PL	3D	7PL	3D	7PL	3D
$f_1-f_2$	166.08	156.34	165.07	155.34	165.93	159.11
$f_3-f_4$	168.36	165.52	167.19	164.37	169.40	162.67
$f_5-f_6$	258.15	247.58	256.59	246.01	263.57	252.32
$f_7-f_8$	330.83	331.02	328.56	328.75	321.87	321.89
$f_9-f_{10}$	368.54	359.67	366.25	357.34	375.09	365.31
$f_{11}$	422.31	419.84	419.00	416.72	412.14	409.15
$f_{12}-f_{13}$	437.11	434.21	433.59	430.96	426.26	422.88
Max. Error	5.87%	-	5.89%	-	4.27%	-

Lastly, from the natural frequencies of hemispherical shells presented in Tables 18–21, it is noted that the maximum relative errors are above the values obtained in the previous comparisons reported here; they are found in a range between 4.27% and 7.95%. The higher values of maximum relative errors occur when a very thick shell is analyzed, i.e.,  $r/h_m = 2.5$ . It must be mentioned that the majority of the maximum relative errors are above 5%.

In addition, Table 22 presents comparisons of the vibration modes obtained using both models (7-PL and 3D) for a hemispherical shell with LVT, CF boundary conditions, and  $n = 5$ . The similarities between models for vibration modes and natural frequencies are noted in these comparisons.

In general, the behavior of natural frequencies is similar to that observed when analyzing thin and thick shells, that is, an increase in the frequencies value is observed when the shells become thicker. In addition, the study cases analyzed in this section demonstrate the behavior of the present model.

**Table 22.** Vibration modes for a hemispherical shell with LVT and CF boundary conditions,  $n = 5$  (FG-I,  $r_0/h_m = 10$ ,  $r_0 = 2$  m,  $\beta = 2$ ,  $\varphi_0 = \pi/2$ ,  $\varphi_1 = \pi/6$ ).

Model	Vibration Mode					
	$f_1-f_2$	$f_3-f_4$	$f_5-f_6$	$f_7-f_8$	$f_9$	$f_{10}-f_{11}$
7-PL	213.72 Hz 	284.29 Hz 	340.23 Hz 	435.41 Hz 	471.54 Hz 	490.25 Hz 
3D	203.73 Hz 	266.47 Hz 	338.50 Hz 	416.22 Hz 	457.11 Hz 	474.15 Hz 

## 8. Conclusions

From the present work, the following conclusions can be drawn:

- A finite element model for the linear vibration analysis, using spectral/ $hp$  elements based on a seven-parameter shell formulation, is extended to study functionally graded shells.
- Comparisons with the numerical results of a simulation using solid elements verify the performance of the present formulation. In addition, the comparisons suggest that the present formulation shows a better behavior for the modeling of conical, cylindrical, and parabolic shells subjected to the boundary conditions considered herein.
- In general, although the relative errors are between 6% and 8% obtained in the study of hemispherical shells, the present formulation has a good behavior for moderately thick to thin shells. It must be recalled that mechanical properties through the thickness of the 3D model are approximated using several layers in this direction. On the other hand, in the studies reported using the present formulation, the variation of the mechanical properties is evaluated using several Gauss-points while numerical integration through thickness is made, resulting in a closer approximation of them. For the aforementioned reasons, some differences between results, but a similar behavior, can be expected.
- Studying the effect of the power-law index on the free vibration response is relevant since, for a given thick or thin shell and boundary conditions, its response may be stiffer or not as the power-law index increases.
- Finally, the spectral/ $hp$  seven-parameter formulation used in the present finite element model allows a straightforward implementation of the FGM behavior and the use of three-dimensional constitutive equations. These features allow the use of considerably fewer elements, and therefore computational time, to model FG shell structures, when compared with models made of solid elements.

**Author Contributions:** Conceptualization, C.E.V.M. and M.E.G.R.; investigation, C.E.V.M. and N.F.S.; software, C.E.V.M., M.E.G.R. and N.F.S.; validation, C.E.V.M.; formal analysis, C.E.V.M., M.E.G.R. and N.F.S.; writing—original draft preparation, C.E.V.M. and M.E.G.R.; writing—review and editing, C.E.V.M., M.E.G.R., N.F.S. and L.D.C.G.; visualization, C.E.V.M. All authors have read and agreed to the published version of the manuscript.

**Funding:** The APC was funded by Instituto de Innovación, Ciencia y Emprendimiento para la Competitividad para el Estado de Guanajuato (IDEAGTO) grant number IDEAGTO/CONV/069/2023.

**Institutional Review Board Statement:** Not applicable.

**Informed Consent Statement:** Not applicable.

**Data Availability Statement:** The data presented in this study are available on request from the corresponding author. The data are not publicly available.

**Conflicts of Interest:** The authors declare no conflict of interest.

## Abbreviations and Nomenclature

The following abbreviations and nomenclature are used in this manuscript:

### Abbreviations

FGM	Functionally graded material
FG	Functionally graded
FSDT	First-order shear deformation theory
TSDT	Third-order shear deformation theory
HSDT	Higher-order shear deformation theory
3D	Three-dimensional
2D	Two-dimensional
FG-I	Volume distribution of top constituent according to Equation (12)
FG-II	Volume distribution of top constituent according to Equation (13)
C	Clamped boundary condition
S	Simply supported boundary condition
F	Free edge boundary condition
UT	Uniform or constant thickness
LVT	Linear variable thickness

### Nomenclature

$\Phi$	3D geometry of the shell element
$\Omega$	Shell's mid-surface
$\zeta^i$	Direction $i$ of the curvilinear coordinates
$p$	Polynomial order
$\psi_k(\zeta^1, \zeta^2)$	2D Lagrange interpolation function of order $p$
$\mathbf{X}^k$	Position vector of $k$ -th spectral node
$\mathbf{n}^k$	Unit normal vector of the $k$ -th spectral node
$h$	Thickness at the $k$ -th spectral node position
$q$	Number of spectral nodes per element
$(\bullet)_{,i}$	First derivative with respect to $\zeta^i$
$\mathbf{g}_i$	Set of covariant basis vectors
$[\mathbf{J}]$	Jacobian matrix
$J$	Determinant of the Jacobian matrix
$\mathbf{g}^i$	Set of contravariant basis vectors
$\mathbf{u}(\zeta^\alpha, t)$	Vector of the mid-surface displacements
$\boldsymbol{\varphi}(\zeta^\alpha, t)$	Difference vector
$\Psi$	Seventh parameter
$\mathbf{E}$	Green–Lagrange strain tensor
$E_{\alpha\beta}$	Strain covariant component
$\varepsilon_{\alpha\beta}^{(0)}$	Strain covariant component associated with constant terms according to $\zeta^3$
$\varepsilon_{\alpha\beta}^{(1)}$	Strain covariant component associated with linear terms according to $\zeta^3$
$n$	Volume fraction exponent or power-law index
$V_{top}^i(\zeta^3)$	Volume distribution of the top constituent following the power-law form $i$
$C^{ijkl}$	Contravariant components of the fourth-order elasticity tensor
$\lambda(\zeta^3), \mu(\zeta^3)$	Lamé parameters as a function of $\zeta^3$
$g^{ij}$	Contravariant components of the Riemannian metric tensor
$(\dot{\bullet})$	Partial derivative with respect to time
$I_i$	Mass inertia
$A^{ijkl}$	Effective extensional fourth-order stiffness tensor component
$B^{ijkl}$	Effective extensional–bending coupling fourth-order stiffness tensor component
$D^{ijkl}$	Effective bending fourth-order stiffness tensor component
$\omega$	Frequency of natural vibration
$\Delta^e$	Vibration mode vector of the element $e$
$h_m$	Average thickness

### Appendix A. Convergence Study

In this appendix, the results of the convergence study performed to determine the mesh size for the numerical comparisons are presented. They were obtained using meshes with seven-parameter elements of order  $p = 8$ . For conical and cylindrical shells with uniform thickness, the geometrical parameters considered are those reported in [22], and for parabolic and hemispherical shells they are those presented in [23].

In the following tables, the label Size indicates the number of elements used for each mesh analyzed in the convergence study, and the mesh sizes considered were 4, 16, 25, and 36. Note that the first mesh size corresponds to a coarse mesh, and the last one corresponds to a fine mesh.

Table A1 presents the convergence study for conical shells with uniform thickness (UT) and linear variable thickness (LVT), and both truncated cones are under CF boundary conditions and their volume distribution is type FG-II; see Equation (13). From the results, it is observed that meshes of 25 elements give a good convergence for the first ten frequencies.

**Table A1.** Convergence of natural frequencies for conical shells with UT and LVT under CF boundary conditions (FG-II).

$n$	Size	Natural Frequency									
		$f_1$	$f_2$	$f_3$	$f_4$	$f_5$	$f_6$	$f_7$	$f_8$	$f_9$	$f_{10}$
UT											
0.6	4	206.3399	206.3406	228.7445	228.7594	307.8573	310.0378	318.3083	318.3083	349.2583	349.2601
	16	206.2043	206.2043	225.9955	225.9955	279.1271	279.1425	318.2458	318.2458	349.0163	349.0163
	25	206.1950	206.1950	225.9754	225.9754	279.0831	279.0831	318.2343	318.2343	348.9862	348.9862
	36	206.1895	206.1895	225.9625	225.9625	279.0604	279.0604	318.2267	318.2267	348.9669	348.9669
1	4	205.2655	205.2661	227.6316	227.6455	306.4297	308.6182	316.4647	316.4647	347.4014	347.4036
	16	205.1328	205.1328	224.9006	224.9006	277.8596	277.8751	316.4039	316.4039	347.1603	347.1603
	25	205.1241	205.1241	224.8809	224.8809	277.8168	277.8168	316.3927	316.3927	347.1300	347.1300
	36	205.1192	205.1192	224.8691	224.8691	277.7954	277.7954	316.3855	316.3855	347.1107	347.1107
5	4	204.3267	204.3273	230.8937	230.9606	309.7112	309.7112	313.8276	316.9194	346.9169	346.9202
	16	204.1959	204.1959	228.1823	228.1823	285.6315	285.6461	309.6502	309.6502	346.6729	346.6729
	25	204.1866	204.1866	228.1618	228.1618	285.5871	285.5871	309.6392	309.6392	346.6426	346.6426
	36	204.1816	204.1816	228.149	228.149	285.5645	285.5645	309.6318	309.6318	346.6229	346.6229
VT											
$\alpha = 60^\circ, r_0/h_m = 5, L/h_m = 10, h_1/h_0 = 2$											
0.6	4	64.2671	64.2683	72.8039	72.8039	77.7359	77.8637	82.4200	111.7707	112.4981	119.3929
	16	64.2381	64.2383	72.7834	72.7834	77.1862	77.1862	82.3982	105.1581	105.1593	119.3415
	25	64.2342	64.2342	72.7792	72.7792	77.1813	77.1813	82.3935	105.1495	105.1496	119.3310
	36	64.2314	64.2316	72.7765	72.7765	77.1782	77.1782	82.3906	105.1451	105.1451	119.3240
1	4	64.0133	64.0147	72.5720	72.5720	77.4079	77.5351	82.1966	111.3054	112.0354	118.9686
	16	63.9856	63.9856	72.5516	72.5516	76.8608	76.8608	82.1739	104.7152	104.7165	118.9188
	25	63.9819	63.9819	72.5476	72.5476	76.8562	76.8562	82.1693	104.7070	104.7070	118.9087
	36	63.9793	63.9793	72.5448	72.5448	76.8531	76.8531	82.1662	104.7027	104.7027	118.9018
5	4	64.7178	64.7191	71.8602	71.8604	79.7390	79.8619	80.9811	114.8458	115.4412	119.9444
	16	64.6894	64.6896	71.8401	71.8401	79.1981	79.1981	80.9595	108.2964	108.2974	119.8919
	25	64.6855	64.6855	71.8360	71.8360	79.1933	79.1933	80.9551	108.2880	108.2880	119.8812
	36	64.6829	64.6829	71.8332	71.8332	79.1901	79.1901	80.9522	108.2835	108.2835	119.8740

The results of the convergence study for cylindrical shells with UT and LVT are presented in Table A2, both of them under CF boundary conditions. From this study, in general, the convergence was observed for a mesh size of 25 elements.

Table A3 shows the convergence of the natural frequencies for parabolic shells under SF boundary conditions, and for several values of the power-law index  $n$ . For uniform thickness, a good convergence was obtained using a mesh size of 16 elements. However, for a parabolic shell with LVT, the convergence was observed at meshes of 25 elements.

**Table A2.** Convergence of natural frequencies for cylindrical shells with UT and with LVT under CF boundary conditions (FG-II).

<i>n</i>	Size	Natural Frequency									
		<i>f</i> <sub>1</sub>	<i>f</i> <sub>2</sub>	<i>f</i> <sub>3</sub>	<i>f</i> <sub>4</sub>	<i>f</i> <sub>5</sub>	<i>f</i> <sub>6</sub>	<i>f</i> <sub>7</sub>	<i>f</i> <sub>8</sub>	<i>f</i> <sub>9</sub>	<i>f</i> <sub>10</sub>
UT											
<i>r/h</i> = 10											
0.6	4	149.0672	149.0813	217.4327	220.1873	250.289	250.289	414.3378	421.2149	422.6686	431.4761
	16	148.9533	148.9533	213.7694	213.7694	250.2324	250.2324	375.1731	375.2126	414.3378	418.8546
	25	148.9471	148.9471	213.7647	213.7647	250.2258	250.2258	375.1441	375.1441	414.3378	418.8213
	36	148.9438	148.9438	213.7629	213.7629	250.2222	250.2222	375.1404	375.1404	414.3378	418.8004
1	4	148.1871	148.2012	216.6958	219.4371	248.6176	248.6176	411.5388	419.159	420.6086	430.1546
	16	148.0766	148.0766	213.0478	213.0478	248.5642	248.5642	374.0646	374.1038	411.5388	416.811
	25	148.0712	148.0712	213.043	213.043	248.5585	248.5585	374.0361	374.0361	411.5388	416.7794
	36	148.0683	148.0683	213.0418	213.0418	248.5555	248.5555	374.0327	374.0327	411.5388	416.7596
5	4	147.6200	147.6372	224.2188	226.9312	242.8096	242.8096	401.1873	424.5701	426.0516	445.3043
	16	147.5116	147.5116	220.4488	220.4488	242.759	242.759	388.7491	388.7856	401.1873	422.1085
	25	147.5064	147.5064	220.4442	220.4442	242.7538	242.7538	388.7211	388.7211	401.1873	422.0764
	36	147.5035	147.5035	220.4425	220.4425	242.7507	242.7507	388.7175	388.7175	401.1873	422.0560
LVT											
<i>r</i> <sub>0</sub> / <i>h</i> <sub><i>m</i></sub> = 5, <i>h</i> <sub><i>m</i></sub> = 3/4, <i>L/h</i> <sub><i>m</i></sub> = 10, <i>h</i> <sub>1</sub> / <i>h</i> <sub>0</sub> = 2											
0.6	4	58.5325	58.5403	79.1170	79.1170	97.4787	98.0998	125.2401	157.4556	157.4597	180.5150
	16	58.5032	58.5035	79.1061	79.1061	96.1520	96.1520	125.2401	157.3938	157.3941	162.9478
	25	58.5015	58.5015	79.1040	79.1040	96.1511	96.1511	125.2401	157.3840	157.3840	162.9408
	36	58.5002	58.5004	79.1026	79.1026	96.1505	96.1505	125.2401	157.3773	157.3774	162.9400
1	4	58.2046	58.2122	78.4490	78.4490	97.2474	97.8640	124.1085	156.6195	156.6236	179.9211
	16	58.1765	58.1767	78.4397	78.4397	95.9248	95.9248	124.1085	156.5594	156.5598	162.6202
	25	58.1750	58.1750	78.4377	78.4377	95.9238	95.9238	124.1085	156.5500	156.5501	162.6132
	36	58.1739	58.1739	78.4366	78.4366	95.9233	95.9234	124.1085	156.5436	156.5437	162.6124
5	4	58.8273	58.8348	76.8844	76.8844	100.5552	101.1290	120.9788	156.7878	156.7918	183.6858
	16	58.7989	58.7991	76.8743	76.8743	99.2149	99.2149	120.9788	156.7283	156.7286	168.2562
	25	58.7974	58.7974	76.8723	76.8723	99.2141	99.2141	120.9788	156.7189	156.7189	168.2494
	36	58.7963	58.7963	76.8710	76.8710	99.2135	99.2137	120.9788	156.7125	156.7126	168.2487

**Table A3.** Convergence of natural frequencies for parabolic shells with UT and LVT under SF boundary conditions (FG-I).

<i>n</i>	Size	Natural Frequency									
		<i>f</i> <sub>1</sub>	<i>f</i> <sub>2</sub>	<i>f</i> <sub>3</sub>	<i>f</i> <sub>4</sub>	<i>f</i> <sub>5</sub>	<i>f</i> <sub>6</sub>	<i>f</i> <sub>7</sub>	<i>f</i> <sub>8</sub>	<i>f</i> <sub>9</sub>	<i>f</i> <sub>10</sub>
UT											
0.6	4	115.0771	115.0783	162.5836	162.5836	163.816	163.8276	190.6016	205.3549	205.3549	205.7548
	16	115.0375	115.0375	162.5828	162.5828	162.6739	162.6739	190.6009	194.7506	194.7545	205.3518
	25	115.0374	115.0374	162.5828	162.5828	162.6739	162.6739	190.6009	194.7454	194.7454	205.3518
	36	115.0373	115.0373	162.5828	162.5828	162.6732	162.6732	190.6009	194.7448	194.7448	205.3518
1	4	114.1884	114.1895	161.5536	161.5536	162.9672	162.9773	189.1796	203.9445	203.9445	204.8127
	16	114.1494	114.1494	161.5521	161.5521	161.8309	161.8309	189.1789	193.8818	193.8857	203.9420
	25	114.1493	114.1493	161.5521	161.5521	161.8301	161.8301	189.1789	193.8772	193.8772	203.9420
	36	114.1492	114.1492	161.5521	161.5521	161.8301	161.8301	189.1789	193.8766	193.8766	203.9420
5	4	114.1847	114.1854	157.9431	157.9431	162.9485	162.9594	186.2609	202.1293	202.1293	206.7551
	16	114.1467	114.1467	157.9423	157.9423	161.8215	161.8215	186.2609	195.7845	195.7884	202.1268
	25	114.1466	114.1466	157.9423	157.9423	161.8207	161.8207	186.2602	195.7800	195.7800	202.1268
	36	114.1465	114.1465	157.9423	157.9423	161.8207	161.8207	186.2602	195.7793	195.7793	202.1262

**Table A3.** Cont.

<i>n</i>	Size	Natural Frequency									
		<i>f</i> <sub>1</sub>	<i>f</i> <sub>2</sub>	<i>f</i> <sub>3</sub>	<i>f</i> <sub>4</sub>	<i>f</i> <sub>5</sub>	<i>f</i> <sub>6</sub>	<i>f</i> <sub>7</sub>	<i>f</i> <sub>8</sub>	<i>f</i> <sub>9</sub>	<i>f</i> <sub>10</sub>
LVT		<i>F/h<sub>m</sub></i> = 5, <i>F</i> = 0.875 m, <i>β</i> = 1.5, <i>φ</i> <sub>0</sub> = <i>π</i> /6, <i>φ</i> <sub>1</sub> = <i>π</i> /3									
0.6	4	139.0314	139.0330	184.2228	184.5964	232.6821	232.6821	273.5517	277.8245	302.1489	302.1493
	16	138.9795	138.9801	181.8076	181.8076	232.6816	232.6816	252.5840	252.5940	302.1124	302.1128
	25	138.9790	138.9790	181.8048	181.8048	232.6810	232.6816	252.5714	252.5714	302.1111	302.1111
	36	138.9782	138.9784	181.8041	181.8041	232.6810	232.6810	252.5694	252.5694	302.1111	302.1116
1	4	137.4007	137.4023	182.9299	183.3013	230.7302	230.7302	271.8826	276.1198	300.6015	300.6019
	16	137.3496	137.3502	180.5318	180.5318	230.7280	230.7280	251.0767	251.0868	300.5687	300.5691
	25	137.3490	137.3490	180.5297	180.5297	230.7280	230.7280	251.0646	251.0646	300.5674	300.5678
	36	137.3481	137.3482	180.5290	180.5290	230.7275	230.7280	251.0626	251.0631	300.5678	300.5678
5	4	136.9053	136.9081	185.7905	186.1861	225.5277	225.5277	276.6422	281.0989	299.3446	299.3454
	16	136.8544	136.8549	183.4657	183.4657	225.5265	225.5265	255.8724	255.8819	299.3099	299.3099
	25	136.8537	136.8538	183.4636	183.4636	225.5260	225.5265	255.8606	255.8606	299.3086	299.3086
	36	136.8530	136.8531	183.4629	183.4629	225.5260	225.5260	255.8591	255.8591	299.3086	299.3091

For several values of the power-law index *n*, Table A4 presents the convergence of the natural frequencies of hemispherical shells with UT and LVT under CF boundary conditions. For both cases, within the first ten frequencies, a good convergence was observed when a mesh of 25 elements was used.

**Table A4.** Convergence of natural frequencies for hemispherical shells with UT and LVT under CF boundary conditions (FG-I).

<i>n</i>	Size	Natural Frequency									
		<i>f</i> <sub>1</sub>	<i>f</i> <sub>2</sub>	<i>f</i> <sub>3</sub>	<i>f</i> <sub>4</sub>	<i>f</i> <sub>5</sub>	<i>f</i> <sub>6</sub>	<i>f</i> <sub>7</sub>	<i>f</i> <sub>8</sub>	<i>f</i> <sub>9</sub>	<i>f</i> <sub>10</sub>
UT											
0.6	4	142.9211	142.9228	208.2505	209.0329	286.9648	286.9648	371.2498	378.0133	379.8979	412.0659
	16	142.7639	142.7639	204.6190	204.6190	286.8809	286.8809	335.2968	335.3127	379.7792	411.9857
	25	142.7490	142.7490	204.6141	204.6141	286.8646	286.8646	335.2817	335.2817	379.7558	411.9716
	36	142.7395	142.7395	204.6122	204.6122	286.8536	286.8536	335.2802	335.2802	379.7405	411.9624
1	4	141.9287	141.9304	206.8133	207.592	284.9687	284.9687	368.682	375.4016	377.1949	409.1480
	16	141.7716	141.7716	203.2066	203.2066	284.8847	284.8847	332.9832	332.9992	377.0763	409.0685
	25	141.7565	141.7565	203.2023	203.2023	284.8682	284.8682	332.9683	332.9683	377.0531	409.0542
	36	141.7468	141.7468	203.2004	203.2004	284.8576	284.8576	332.9668	332.9668	377.0377	409.0449
5	4	141.5049	141.5083	211.0865	211.8818	278.8679	278.8679	370.0573	372.969	379.5433	401.4401
	16	141.3544	141.3544	207.5792	207.5792	278.7852	278.7852	338.3654	338.3804	369.9389	401.3587
	25	141.3400	141.3400	207.5749	207.5749	278.7689	278.7689	338.3516	338.3516	369.9159	401.3441
	36	141.3306	141.3306	207.5731	207.5731	278.7584	278.7584	338.3505	338.3505	369.9005	401.3347
LVT		<i>r</i> <sub>0</sub> / <i>h<sub>m</sub></i> = 10, <i>r</i> <sub>0</sub> = 2 m, <i>β</i> = 2, <i>φ</i> <sub>0</sub> = <i>π</i> /2, <i>φ</i> <sub>1</sub> = <i>π</i> /6									
0.6	4	213.8630	213.8719	282.1387	283.0775	348.9506	348.9506	465.8914	475.1184	479.0508	496.9698
	16	213.7054	213.7054	278.8270	278.8270	348.8689	348.8689	428.3164	428.3294	478.9194	496.8319
	25	213.6865	213.6865	278.8166	278.8166	348.8526	348.8526	428.2966	428.2966	478.8930	496.8067
	36	213.6740	213.6740	278.8107	278.8107	348.8417	348.8417	428.2918	428.2918	478.8750	496.7901
1	4	212.2336	212.2425	280.1837	281.1138	346.3059	346.3059	462.5427	471.6680	474.5570	492.2946
	16	212.0760	212.0760	276.8967	276.8967	346.2251	346.2251	425.2914	425.3042	474.4270	492.1577
	25	212.0569	212.0569	276.8862	276.8862	346.2086	346.2086	425.2717	425.2717	474.4008	492.1327
	36	212.0443	212.0443	276.8807	276.8807	346.1977	346.1977	425.2672	425.2672	474.3832	492.1162
5	4	213.8920	213.9015	287.5137	288.4290	340.3234	340.3234	471.6913	472.2575	480.9917	490.4160
	16	213.7380	213.7380	284.2981	284.2981	340.2437	340.2437	435.4306	435.4425	471.5627	490.2747
	25	213.7191	213.7191	284.2879	284.2879	340.2277	340.2277	435.4117	435.4117	471.5366	490.2486
	36	213.7066	213.7066	284.2821	284.2821	340.2169	340.2169	435.4067	435.4067	471.5192	490.2313



## References

1. Shen, H.S. *Functionally Graded Materials: Nonlinear Analysis of Plates and Shells*; CRC Press: Boca Raton, FL, USA, 2016.
2. Mahamood, R.M.; Akinlabi, E.T. Introduction to functionally graded materials. In *Functionally Graded Materials*; Springer: Berlin/Heidelberg, Germany, 2017; pp. 1–8.
3. Gupta, A.; Talha, M. Recent development in modeling and analysis of functionally graded materials and structures. *Prog. Aerosp. Sci.* **2015**, *79*, 1–14. [[CrossRef](#)]
4. Punera, D.; Kant, T. A critical review of stress and vibration analyses of functionally graded shell structures. *Compos. Struct.* **2019**, *210*, 787–809. [[CrossRef](#)]
5. Jha, D.K.; Kant, T.; Singh, R.K. A critical review of recent research on functionally graded plates. *Compos. Struct.* **2013**, *96*, 833–849. [[CrossRef](#)]
6. Zhou, W.; Ai, S.; Chen, M.; Zhang, R.; He, R.; Pei, Y.; Fang, D. Preparation and thermodynamic analysis of the porous ZrO<sub>2</sub>/(ZrO<sub>2</sub> + Ni) functionally graded bolted joint. *Compos. Part B Eng.* **2015**, *82*, 13–22. [[CrossRef](#)]
7. Zhou, W.; Ai, S.; He, R.; Pei, Y.; Fang, D. Load distribution in threads of porous metal–ceramic functionally graded composite joints subjected to thermomechanical loading. *Compos. Struct.* **2015**, *134*, 680–688. [[CrossRef](#)]
8. Sofiyev, A.H. A review of reasearch on the vibration and buckling of the FGM conical shells. *Compos. Struct.* **2019**, *211*, 301–317. [[CrossRef](#)]
9. Dong, C.Y. Three-dimensional free vibration analysis of functionally graded annular plates using the Chebyshev–Ritz method. *Mater. Des.* **2008**, *29*, 1518–1525. [[CrossRef](#)]
10. Talha, M.; Singh, B.N. Static response and free vibration analysis of FGM plates using higher order shear deformation theory. *Appl. Math. Model.* **2010**, *34*, 3991–4011. [[CrossRef](#)]
11. Neves, A.M.A.; Ferreira, A.J.M.; Carrera, E.; Cinefra, M.; Roque, C.M.C.; Jorge, R.M.N.; Soares, C.M. Static, free vibration and buckling analysis of isotropic and sandwich functionally graded plates using a quasi-3D higher-order shear deformation theory and a meshless technique. *Compos. Part B Eng.* **2013**, *44*, 657–674. [[CrossRef](#)]
12. Thai, H.T.; Vo, T.P. A new sinusoidal shear deformation theory for bending, buckling, and vibration of functionally graded plates. *Appl. Math. Model.* **2013**, *37*, 3269–3281. [[CrossRef](#)]
13. Ramu, I.; Mohanty, S.C. Modal analysis of functionally graded material plates using finite element method. *Procedia Mater. Sci.* **2014**, *6*, 460–467. [[CrossRef](#)]
14. Ghashochi-Bargh, H.; Razavi, S. A simple analytical model for free vibration of orthotropic and functionally graded rectangular plates. *Alex. Eng. J.* **2018**, *57*, 595–607. [[CrossRef](#)]
15. Katili, I.; Batoz, J.L.; Maknun, I.J.; Katili, A.M. On static and free vibration analysis of FGM plates using an efficient quadrilateral finite element based on DSPM. *Compos. Struct.* **2021**, *261*, 113514. [[CrossRef](#)]
16. Vinh, P.V.; Dung, N.T.; Tho, N.C.; Thom, D.V.; Hoa, L.K. Modified single variable shear deformation plate theory for free vibration analysis of rectangular FGM plates. *Structures* **2021**, *29*, 1435–1444. [[CrossRef](#)]
17. Wang, X.; Jin, C.; Yuan, Z. Free vibration of FGM annular sectorial plates with arbitrary boundary supports and large sector angles. *Mech. Based Des. Struct. Mach.* **2022**, *50*, 331–351. [[CrossRef](#)]
18. Efraim, E.; Eisenberger, M. Exact vibration analysis of variable thickness thick annular isotropic and FGM plates. *J. Sound Vib.* **2007**, *299*, 720–738. [[CrossRef](#)]
19. Temel, B.; Noori, A.R. A unified solution for the vibration analysis of two-directional functionally graded axisymmetric Mindlin–Reissner plates with variable thickness. *Int. J. Mech. Sci.* **2020**, *174*, 105471. [[CrossRef](#)]
20. Kumar, V.; Singh, S.J.; Saran, V.H.; Harsha, S.P. An analytical framework for rectangular FGM tapered plate resting on the elastic foundation. *Mater. Today Proc.* **2020**, *28*, 1719–1726. [[CrossRef](#)]
21. Matsunaga, H. Free vibration and stability of functionally graded circular cylindrical shells accorinding to a 2D higher-order deformation theory. *Compos. Struct.* **2009**, *88*, 519–531. [[CrossRef](#)]
22. Tornabene, F.; Viola, E.; Inman, D.J. 2-D differential quadrature solution for vibration analysis of functionally graded conical, cylindrical shell and annular plate structures. *J. Sound Vib.* **2009**, *328*, 259–290. [[CrossRef](#)]
23. Tornabene, F.; Viola, E. Free vibration analysis of functionally graded panels and shells of revolution. *Meccanica* **2009**, *44*, 255–281. [[CrossRef](#)]
24. Iqbal, Z.; Naeem, M.N.; Sultana, N. Vibration characteristics of FGM circular cylindrical shells using wave propagation approach. *Acta Mech.* **2009**, *208*, 237–248. [[CrossRef](#)]
25. Neves, A.M.A.; Ferreira, A.J.M.; Carrera, E.; Cinefra, M.; Roque, C.M.C.; Jorge, R.M.N.; Soares, C.M.M. Free vibration analysis of functionally graded shells by a higher-order shear deformation theory and radial basis functions collocation, accounting for through-the-thickness deformations. *Eur. J. Mech. A/Solids* **2013**, *37*, 24–34. [[CrossRef](#)]
26. Su, Z.; Jin, G.; Shi, S.; Ye, T. A unified accurate solution for vibration analysis of arbitrary functionally graded spherical shell segments with general boundary conditions. *Compos. Struct.* **2014**, *111*, 271–284. [[CrossRef](#)]
27. Su, Z.; Jin, G.; Shi, S.; Ye, T.; Jia, X. A unified solution for vibration analysis of functionally graded cylindrical, conical shells and annular plates with general boundary conditions. *Int. J. Mech. Sci.* **2014**, *80*, 62–80. [[CrossRef](#)]
28. Su, Z.; Jin, G.; Ye, T. Three-dimensional vibration analysis of thick functionally graded conical, cylindrical shell and annular plate structures with arbitrary elastic restraints. *Compos. Struct.* **2014**, *118*, 432–447. [[CrossRef](#)]

29. Torabi, J.; Ansari, R. A higher-order isoparametric superelement for free vibration analysis of functionally graded shells of revolution. *Thin-Walled Struct.* **2018**, *133*, 169–179. [[CrossRef](#)]
30. Ersoy, H.; Mercan, K.; Civalek, Ö. Frequencies of FGM shells and annular plates by the methods of discrete singular convolution and differential quadrature methods. *Compos. Struct.* **2018**, *183*, 7–20. [[CrossRef](#)]
31. Brischetto, S. Exponential matrix method for the solution of exact 3D equilibrium equations for free vibrations of functionally graded plates and shells. *J. Sandw. Struct. Mater.* **2019**, *21*, 77–114. [[CrossRef](#)]
32. Pham, T.D.; Pham, Q.H.; Phan, V.D.; Nguyen, H.N.; Do, V.T. Free vibration analysis of functionally graded shells using an edge-based smoothed finite element method. *Symmetry* **2019**, *11*, 684. [[CrossRef](#)]
33. Moita, J.S.; Araújo, A.L.; Correia, V.F.; Mota Soares, C.a.M. Vibrations of Functionally Graded Material Axisymmetric Shells. *Compos. Struct.* **2020**, *248*, 112489. [[CrossRef](#)]
34. Zannon, M.; Abu-Rqayiq, A.; Al-bdour, A. Free vibration analysis of thick FGM spherical shells based on a third-order shear deformation theory. *Eur. J. Pure Appl. Math.* **2020**, *13*, 766–778. [[CrossRef](#)]
35. Bagheri, H.; Kiani, Y.; Eslami, M.R. Free vibration of FGM conical–spherical shells. *Thin-Walled Struct.* **2021**, *160*, 107387. [[CrossRef](#)]
36. Li, H.; Pang, F.; Gong, Q.; Teng, Y. Free vibration analysis of axisymmetric functionally graded doubly-curved shells with un-uniform thickness distribution based on Ritz method. *Compos. Struct.* **2019**, *225*, 111145. [[CrossRef](#)]
37. Gong, Q.; Li, H.; Chen, H.; Teng, Y.; Wang, N. Application of Ritz method for vibration analysis of stepped functionally graded spherical torus shell with general boundary conditions. *Compos. Struct.* **2020**, *243*, 112215. [[CrossRef](#)]
38. Tornabene, F.; Fantuzzi, N.; Bacciocchi, M. Free vibrations of free-form doubly-curved shells made of functionally graded materials using higher-order equivalent single layer theories. *Compos. Part B Eng.* **2014**, *67*, 490–509. [[CrossRef](#)]
39. Tornabene, F.; Fantuzzi, N.; Bacciocchi, M.; Viola, E.; Reddy, J.N. A numerical investigation on the natural frequencies of FGM sandwich shells with variable thickness by the Local Generalized Differential Quadrature Method. *Appl. Sci.* **2017**, *7*, 131. [[CrossRef](#)]
40. Rao, D.K.; Blessington, P.J.; Tarapada, R. Finite Element Modeling and Analysis of Functionally Graded (FG) Composite Shell Structures. *Procedia Eng.* **2012**, *38*, 3192–3199. [[CrossRef](#)]
41. Mouli, B.C.; Kar, V.; Ramji, K.; Rajesh, M. Free vibration of functionally graded conical shell. *Mater. Today Proc.* **2018**, *5*, 14302–14308. [[CrossRef](#)]
42. Marzavan, S.; Nastasescu, V. Free vibration analysis of a functionally graded plate by finite element method. *Ain Shams Eng. J.* **2023**, *14*, 102024. [[CrossRef](#)]
43. Burlayenko, V.N.; Sadowski, T.; Altenbach, H.; Dimitrova, S. Three-Dimensional Finite Element Modelling of Free Vibrations of Functionally Graded Sandwich Panels. In *Recent Developments in the Theory of Shells*; Springer: Berlin/Heidelberg, Germany, 2019; pp. 157–177.
44. Bischoff, M.; Ramm, E. Shear deformable shell elements for large strains and rotations. *Int. J. Numer. Methods Eng.* **1997**, *40*, 4427–4449. [[CrossRef](#)]
45. Hahn, Y.; Kikuchi, N. Mixed shell element for seven-parameter formulation. *Int. J. Numer. Methods Eng.* **2005**, *64*, 95–124. [[CrossRef](#)]
46. Arciniega, R.A.; Reddy, J.N. Tensor-based finite element formulation for geometrically nonlinear analysis of shell structures. *Comput. Methods Appl. Mech. Eng.* **2007**, *196*, 1048–1073. [[CrossRef](#)]
47. Payette, G.S.; Reddy, J.N. A seven-parameter spectral/hp finite element formulation for isotropic, laminated composite and functionally graded shell structures. *Comput. Methods Appl. Mech. Eng.* **2014**, *278*, 664–704. [[CrossRef](#)]
48. Gutierrez Rivera, M.; Reddy, J.N. Stress analysis of functionally graded shells using a 7-parameter shell element. *Mech. Res. Commun.* **2016**, *78*, 60–70. [[CrossRef](#)]
49. Valencia Murillo, C.; Gutierrez Rivera, M.; Reddy, J.N. Linear Vibration Analysis of Shells Using a Seven-Parameter Spectral/hp Finite Element Model. *Appl. Sci.* **2020**, *10*, 5102. [[CrossRef](#)]
50. Sansour, C. A theory and finite element formulation of shells at finite deformations involving thickness change: Circumventing the use of a rotation tensor. *Arch. Appl. Mech.* **1995**, *65*, 194–216. [[CrossRef](#)]
51. Praveen, G.N.; Reddy, J.N. Nonlinear transient thermoelastic analysis of functionally graded ceramic-metal plates. *Int. J. Solids Struct.* **1998**, *35*, 4457–4476. [[CrossRef](#)]
52. Reddy, J.N. *Energy Principles and Variational Methods in Applied Mechanics*, 2nd ed.; John Wiley & Sons: Hoboken, NJ, USA, 2002.
53. Reddy, J.N. *An Introduction to the Finite Element Method*, 3rd ed.; McGraw-Hill: New York, NY, USA, 2005.
54. Guennebaud, G.; Jacob, B.; Avery, P.; Bachrach, A.; Barthelémy, S. Eigen v3. 2010. Available online: <http://eigen.tuxfamily.org> (accessed on 24 September 2023).
55. Leissa, A.W.; Kang, J.H. Three-dimensional vibration analysis of paraboloidal shells. *JSME Int. J. Ser. Mech. Syst. Mach. Elem. Manuf.* **2002**, *45*, 2–7. [[CrossRef](#)]

**Disclaimer/Publisher’s Note:** The statements, opinions and data contained in all publications are solely those of the individual author(s) and contributor(s) and not of MDPI and/or the editor(s). MDPI and/or the editor(s) disclaim responsibility for any injury to people or property resulting from any ideas, methods, instructions or products referred to in the content.